Nuclear Inst. and Methods in Physics Research, A 1021 (2022) 165930

Contents lists available at ScienceDirect

Nuclear Inst. and Methods in Physics Research, A

journal homepage: www.elsevier.com/locate/nima

SuperKEKB beam final focus superconducting magnet system

N. Ohuchi [a,*], Y. Arimoto [a], K. Akai [a], K. Aoki [a], N. Higashi [a], K. Kanazawa [a], M. Kawai [a], T. Kawamoto [a], H. Koiso [a], Y. Kondou [a], M. Masuzawa [a], A. Morita [a], S. Nakamura [a], Y. Ohnishi [a], Y. Ohsawa [a], K. Oide [a], N. Okada [a], T. Oki [a], H. Sugimoto [a], M. Tawada [a], K. Tsuchiya [a], R. Ueki [a], X. Wang [a], H. Yamaoka [a], Z. Zong [a], B. Parker [b], M. Anerella [b], J. Escallier [b], A. Ghosh [b,1], H. Hocker [b], A. Jain [b,2], A. Marone [b], P. Wanderer [b,1], J. DiMarco [c], J. Nogiec [c], M. Tartaglia [c], G. Velev [c]

[a] High Energy Accelerator Research Organization (KEK), 1-1 Oho Tsukuba, Ibaraki 305-0801, Japan
[b] Brookhaven National Laboratory (BNL), PO Box 5000, Upton, NY 11973-5000, USA
[c] Fermi National Accelerator Laboratory (FNAL), PO Box 500, Batavia, IL 60510-5011, USA

ARTICLE INFO

Keywords:
SuperKEKB
Beam interaction
Beam final focus
Superconducting magnet
Cryostat
Cryogenics

ABSTRACT

The SuperKEKB was designed and constructed as the upgraded accelerator of KEKB. In this accelerator design, the nano-beam scheme of collision was applied and a luminosity of 8×10^{35} $cm^{-2}s^{-1}$ was targeted. In the design, the beam final focus system was the key component in the accelerator hardware elements. This final focus system consists of 55 superconducting magnets. In this paper, the designs of the magnets, the cryostats and the cryogenic system are shown, and the field measurement results are reported. The SuperKEKB beam operation with the final focus system started on 2018 March 19, and the magnet quench events up to 2020 December 16 are described.

1. Introduction

The SuperKEKB electron–positron collider [1] is the upgraded accelerator of KEKB [2]. The collider consists of two main rings of electron (e^-) and positron (e^+), HER and LER, respectively. It was designed to search for new physics phenomena beyond the Standard Model of particle physics in the B meson regime. The luminosity with 8 GeV e^- and 3.5 GeV e^+ beams at KEKB reached the value of 2.1×10^{34} $cm^{-2}s^{-1}$ on June 17, 2009 [3]. In SuperKEKB with 7 GeV e^- and 4 GeV e^+ beams, the luminosity at 8×10^{35} $cm^{-2}s^{-1}$ was designed as the target of the machine. The luminosity is 40 times higher than the value reached in KEKB. SuperKEKB was designed as the next generation machine based on the nano-beam scheme collision [4] with the beam size of 50 nm in the vertical direction and 10 μm in the horizontal direction, and a beam crossing angle of 83 mrad at the Interaction Point (IP).

For squeezing the beams at the IP and fine beam tuning, the beam final focus system at the Interaction Region (IR) consists of 8 superconducting (SC) main quadrupole magnets, 4 SC compensation solenoid magnets and 43 SC corrector magnets [5].

In this paper, we describe (1) the system configuration of the SuperKEKB final focus system, (2) the design of the SC magnets, (3) the measured field performance of the SC magnets including the magnetic alignment, (4) the magnet-cryostat and the cryogenic system, (5) the quench events from March 19, 2018 to December 16, 2020 and (6) the conclusion.

2. System configuration of the beam final focus system

In the SuperKEKB, the process of final focusing the e^- and e^+ beams at IP is performed with doublets of the main SC quadrupole magnets per IP side and per beam. Therefore 8 main SC quadrupole magnets were placed in the IR. In addition, another 47 SC magnets were placed in the IR, so the total number of the SC magnets is 55. The left and right cryostats, QCS-L and QCS-R with respect to the IP contained 25 and 30 magnets, respectively. Fig. 1 shows the system layout of the SC magnets in the two cryostats.

In this paper, a_n and b_n are the *2n-th* multipole magnet or the normalized magnetic field coefficient with respect to the main field, respectively, at the reference radius, R_{ref}, where magnetic field quality of each magnet is defined for beam operation. A_n and B_n are the skew and normal magnetic field amplitudes of the *2n-th* pole at R_{ref}, respectively.

* Corresponding author.
E-mail address: norihito.ohuchi@kek.jp (N. Ohuchi).
[1] Retired.
[2] A. Jain was with BNL, Upton NY 11973-5000, and he is now with Argonne National Laboratory, Argonne IL 0439 USA.

https://doi.org/10.1016/j.nima.2021.165930
Received 22 July 2021; Received in revised form 11 October 2021; Accepted 12 October 2021
Available online 23 October 2021
0168-9002/© 2021 The Authors. Published by Elsevier B.V. This is an open access article under the CC BY-NC-ND license (http://creativecommons.org/licenses/by-nc-nd/4.0/).

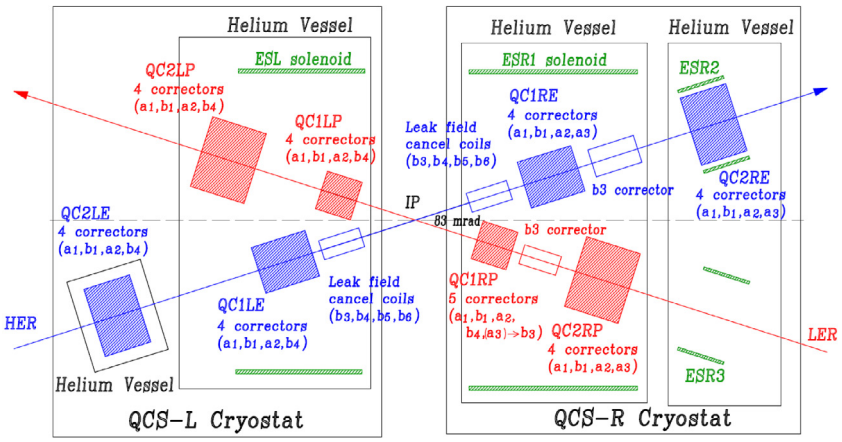

Fig. 1. Conceptual magnet layout in two cryostats.

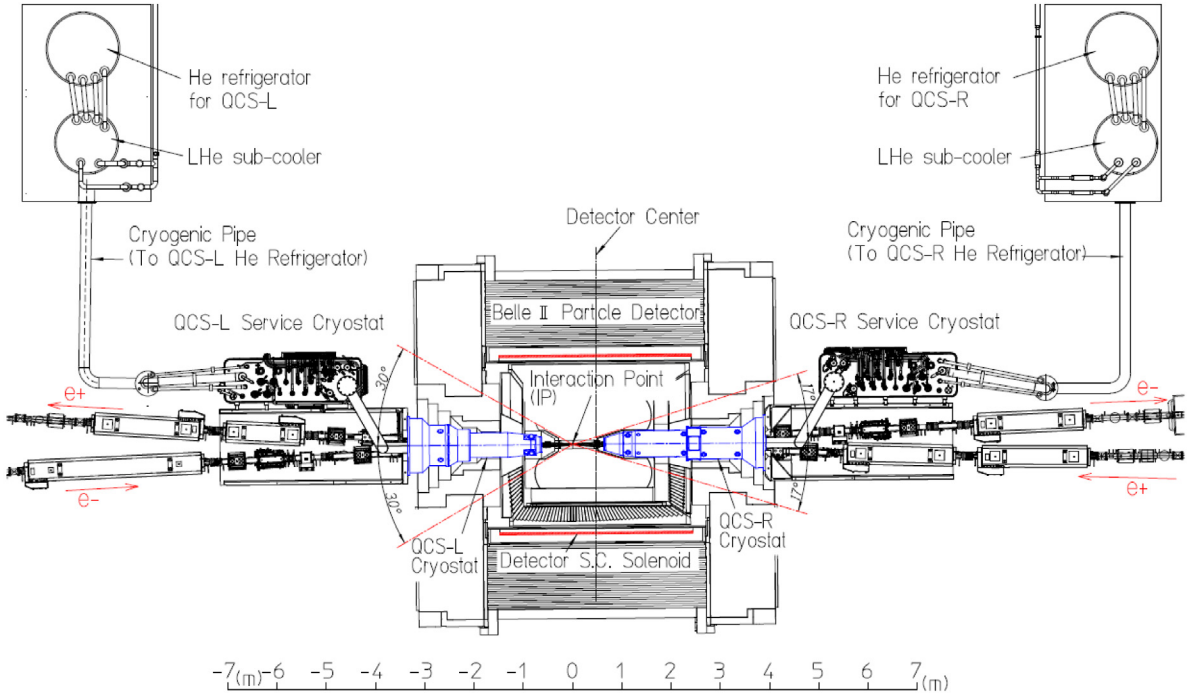

Fig. 2. Top view of the SC magnet cryostats with the cryogenic system, accelerator components in the SuperKEKB interaction region and the horizontal cut view of the Belle II detector. In the figure, the position of zero on the scale is the beam interaction point.

Table 1
The SC magnets for the final focus system.

	Main quadrupole magnet	Corrector magnet	QC1P leak field cancel magnet	Solenoid magnet
QCS-L	QC1LP QC2LP QC1LE QC2LE	a_1,b_1,a_2,b_4 a_1,b_1,a_2,b_4 a_1,b_1,a_2,b_4 a_1,b_1,a_2,b_4	b_3,b_4,b_5,b_6	ESL
QCS-R	QC1RP QC2RP QC1RE QC2RE QC1-2RP QC1-2RE	$a_1,b_1,a_2,\ a_3(b_3),b_4$ a_1,b_1,a_2,a_3 a_1,b_1,a_2,a_3 a_1,b_1,a_2,a_3 b_3 b_3	b_3,b_4,b_5,b_6	ESR1 ESR2 ESR3
Num.	8	35	8	4
Num.			55	

QC1-2RP and QC1-2RE mean the space between two quadrupole magnets. Type of corrector: a_1/b_1 =skew /normal dipole, a_2=skew quadrupole, a_3/b_3=skew/normal sextupole, b_4=normal octupole, b_5=normal decapole, b_6=normal dodecapole.

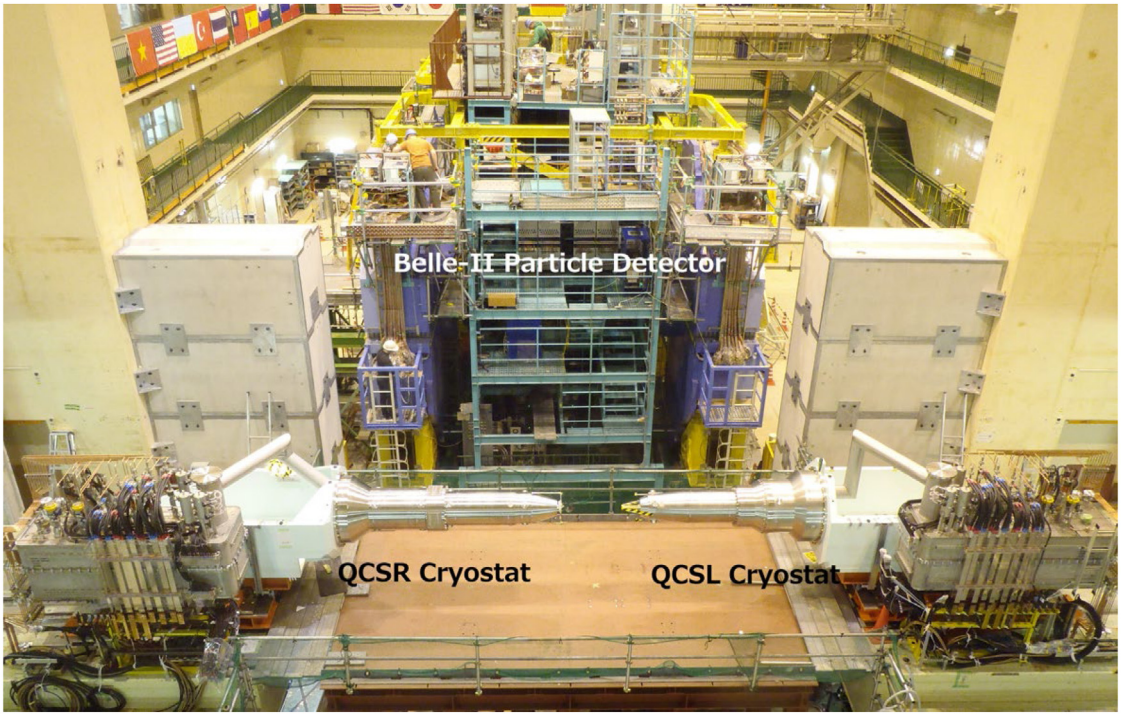

Fig. 3. QCS-R and QCS-L cryostats and Belle-II particle detector at the SuperKEKB IR. The picture was taken after setting two cryostats in the IR and before setting the Belle-II detector along the beam lines.

The 55 SC magnets are classified into three types: (1) 8 main quadrupole magnets [6,7] for focusing or defocusing beams, (2) 35 corrector magnets [8–10] for tuning beams, 8 magnets for canceling the leak field from the main quadrupole magnets and (3) 4 compensation solenoid magnets [11], ESL and ESR1/2/3, for canceling the detector solenoid field at 1.5 T [12]. The SC magnets are installed in two liquid helium (LHe) vessels in each cryostat, as shown in Fig. 1. All magnets are listed in Table 1.

The SC quadrupole magnets for LER, QC1RP and QC1LP, are placed at the closest positions to the IP, and the magnets focus the e^+ beam vertically. The QC2RP and QC2LP are placed outboard (with respect to the IP) of QC1RP and QC1LP, and they focus the e+ beam horizontally. In the same way, QC1LE and QC1RE focus the e^- beam vertically, and QC2RE and QC2LE focus the e^- beam horizontally. The QC2RE and QC2LE magnets are assembled in a separate helium vessel.

Each SC quadrupole magnet has 4 or 5 SC corrector magnets in the magnet bore or on the magnet outer circumference. Two corrector magnets are located between the main quadrupoles in QCS-R.

ESL and ESR1 are assembled in individual cryostats in the helium vessels close to the IP. ESR2 and ESR3 are placed along the e^- and e^+ beam lines, respectively. Both are in the outboard helium vessel in the QCS-R cryostat, respectively.

Fig. 2 shows the top view of the accelerator components including the cryogenic system in the IR and the horizontal cut view of the Belle II detector. The two cryostats are installed completely inside the detector. The IP and the center of the Belle II detector have a shift of 470 mm along the Belle solenoid axis. The SC solenoid of the detector generates a magnetic field at 1.5 T at the detector center, and therefore the 55 SC magnets are designed to be operated under this solenoid field. In the figure, the support stages of two cryostats, the service cryostats and the cryogenic system are shown. The service cryostats have the current leads and the connection ports for the cryogenic transfer tubes. The normal conducting magnets and the beam pipes along the e^- and e^+ beam lines in the IR are shown in this figure. In Table 2, the main parameters of the system are shown. The detailed parameters of the components are described in each section. Fig. 3 shows the QCS-R and QCS-L cryostats and the Belle-II particle detector. The photo was viewed from the outside of the accelerator main ring, and then the positions of the cryostats are opposite to those in Fig. 2.

Table 2
Main parameters of the final focus system.

Number of SC magnets	55
Main quadrupole	Integral field
QC1RP, QC1LP	22.96 T, 22.96 T
QC2RP, QC2LP	11.54 T, 11.48 T
QC1RE, QC1LE	25.39 T, 26.94 T
QC2RE, QC2LE	13.04 T, 15.27 T
Compensation solenoid	Integral field
ESR1 + ESR2 or ESR3	3.86 T•m
ESL	2.31 T•m
Magnet-cryostat	2 units
	Cold mass @ 4 K
QCS-R, QCS-L	3,139 kg, 1,522 kg
He refrigerator cryogenic system	2 units
Cooling power of one unit	250 W @ 4.5 K

3. Design of superconducting magnets

3.1. Constraint conditions of SC magnet design

(a) Space and temperature constraints in the magnet-cryostat design

In the beginning stage of designing the SC quadrupole magnets, the space boundary between the accelerator components and the detector components was strictly defined to be the same as that between Belle and KEKB (the former detector and accelerator) for advancing the design of the machine-detector interface. For the physics experiment, boundary surfaces which have the angle of 17 degrees and 30 degrees for the right and left side with respect to the Belle II solenoid axis were defined as shown in Fig. 2. The positions of the front circular cone surfaces of the QCS-R and QCS-L magnet cryostats are shifted from the boundary surfaces by 233 mm and -402 mm, respectively. Under this space constraint, QC1P and QC1E magnets were required to be positioned as close to the IP as possible. The beam pipes in the two cryostats were designed to be at room temperature.

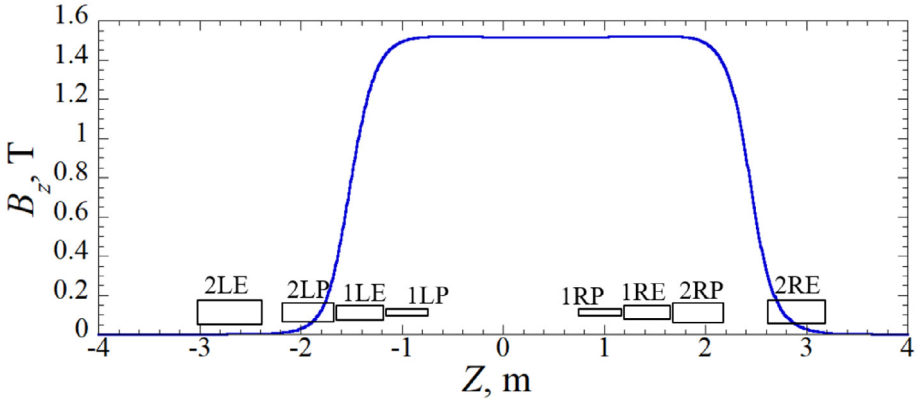

Fig. 4. Calculated magnetic field profile along the Belle II SC solenoid magnet. Z=0 corresponds to the IP position. The axial center of the solenoid magnet is located at Z=0.47 m. The quadrupole magnets with the distance from the IP are shown by the rectangle boxes.

(b) Background magnetic field profile in the IR

The Belle II SC solenoid magnet generates a magnetic field at 1.5 T along the beam lines inside the detector. The solenoid magnetic field profile is shown in Fig. 4. The beam collision point is located at Z=0 m in Fig. 4. This solenoid magnetic field, the beam crossing angle of 83 mrad and the beam focusing process induce an X–Y coupling of e^- and e^+ beams at the IP. The SC quadrupole magnets are shown in the figure with the distance from the IP.

As shown in Figs. 2 and 4, both magnet cryostats are installed inside the Belle II detector and they are operated under the solenoid field. For beam operation, this solenoid field is integrally canceled in each side with respect to the IP by ESL, and ESR1, ESR2 and ESR3.

3.2. Magnetic design of the beam final focus system

As described in the design of the final focus system, the final focus quadrupole magnets are operated in the solenoid field of 1.5 T by the Belle II solenoid. The solenoid field on the beam lines is required to be integrally canceled in each side with respect to the IP with the compensation solenoids.

The six quadrupole magnets of QC1L/RE, QC2L/RE and QC2L/RP have magnetic yokes for reducing the leak field from these magnets to the opposite beam line which is an adjacent beam line in the cryostat. The Belle II solenoid field at 1.5 T is locally canceled by the compensation solenoids for the magnetic yokes not to be in magnetic saturation. The beam pipes on the opposite beam line for the six magnets have magnetic shields against the leak fields from the quadrupole magnets. By the design of the magnetic components, the solenoid fields along the beam lines for the magnets and the opposite beam lines are reduced to be close to zero.

In the space between the IP to QC1LP and QC1RP, the integral field of Belle II solenoid is canceled by the compensation solenoids which are overlaid on the QC1LP and QC1RP. Therefore, QC1LP and QC1RP do not have magnetic yokes. Because the space between two beams and in the front area of the cryostat close to the IP is quite limited, the leak field from QC1LP and QC1RP through the opposite beam pipes (HER) is canceled by special cancel magnets. The sextupole, octupole, decapole and dodecapole cancel magnets are assembled along the HER beam line to do this.

The errors of the quadrupole magnetic center and mid-plane angle are individually adjusted with the a_1, b_1 and a_2 corrector magnets inside of the quadrupole magnet bore.

3.3. Final focus quadrupole magnets

The final focus quadrupole magnets are designed to be located at the specified position due to the tight requirement of beam optics. The quadrupole magnets on the LER beam line are rolled with a specified angle for each magnet because of the combined solenoid field profiles of the Belle II solenoid and ESL and ESR1/2/3. The field centers of all quadrupole magnets have deliberate design offsets in the vertical direction with respect to straight lines through the IP which have a crossing angle of 83 mrad. The axes of the magnetic centers for the HER quadrupole magnets have a design offset in the horizontal direction, and the mid-planes are not rotated.

Table 3
Optical requirement of the SC quadrupoles.

Magnet	Int. field T	Z m	Δx mm	Δy mm	Δθ mrad
QC1LP	22.96	−935	0.0	−1.5	−13.35
QC1RP	22.96	935	0.0	−1.0	7.204
QC2LP	11.48	−1925	0.0	−1.5	−3.725
QC2RP	11.54	1925	0.0	−1.0	−2.114
QC1LE	26.94	−1410	0.7	0.0	0.0
QC1RE	25.39	1410	−0.7	0.0	0.0
QC2LE	15.27	−2700	0.7	0.0	0.0
QC2RE	13.04	2925	−0.7	0.0	0.0

where Int. field: integral field gradient, Z: distance from IP to the longitudinal magnetic center on a straight line through the IP, Δx: horizontal design offset of the magnetic center with respect to a straight line through the IP, Δy: vertical design offset of the magnetic center, $\Delta\theta$: roll angle of the mid-plane of the quadrupole field with respect to the horizontal plane.

Their parameters are listed in Table 3. The cross-sections of the quadrupole magnets were designed to fit the beam size along the beam line.

(a) QC1RP and QC1LP quadrupole magnets

Of the eight quadrupoles, the QC1RP and QC1LP magnets [6] are designed to be located at the position closest to the IP. In Fig. 5, the cross-section design of the QC1RP and QC1LP at the magnet longitudinal center is shown along with the corrector magnets and beam pipe.

The design of the quadrupole magnets is based on the concept of the cos 2θ current profile magnet and the double pancake coil configuration. QC1LP and QC1RP do not have magnetic yoke because the combined solenoid fields by the ESL, ESR1 and Belle II solenoids overlay the magnetic field generated by QC1RP and QC1LP.

QC1RP and QC1LP have identical design magnet parameters, as listed in Table 4. The design field gradient and current of the magnets (G_d and I_d) were specified for the beam operation at the colliding energy of 12 GeV in the future. The operation current (I_o) in the table is for the physics experiment at 11 GeV, and then the indicated values are smaller than the design current. In designing the magnets, the load line ratio at 4.7 K was specified to be smaller than 75%. The temperature of 4.7 K is chosen because sub-cooled liquid helium at 0.16 MPa to cool the magnets changes from single phase liquid to two-phase liquid at 4.75 K. In the thermal design, the magnets are cooled with

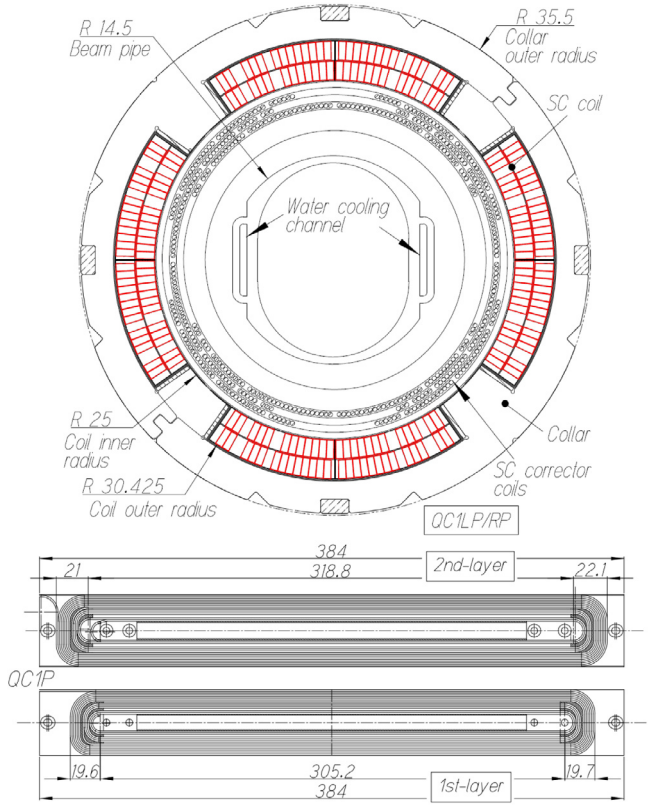

Fig. 5. Cross section and coil design of QC1RP/QC1LP.

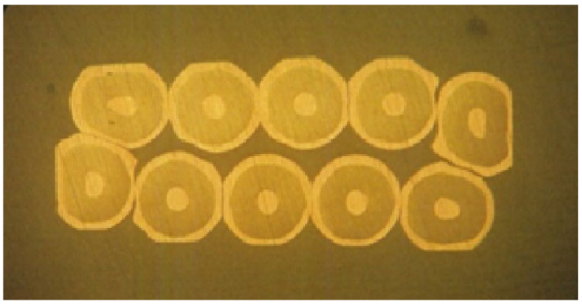

Fig. 6. Cross section of the SC cable for QC1RP/LP.

only liquid helium. This parameter definition is the same for the other main quadrupole magnets. The magnets were designed as a collared magnet, and the outer radius is 35.5 mm. The innermost and outermost radii of the coils are 25 mm and 30.75 mm, respectively. QC1RP and QC1LP are operated under the combined solenoid field of the Belle II solenoid, ESR1 and ESL. The peak magnetic field in the coil (B_p) is the summation of the solenoid field and the magnetic field of QC1LP or QC1RP. In the case of QC1LP, the field strength of ESL at the QC1LP coil produces the peak magnetic field which is $B_z = 2.60\ T$ and $B_r = 1.05$ T. At the operating temperature of 4.7 K, the currents of QC1RP and QC1LP which reach the superconducting critical surface are 2490 A. This current is evaluated with the test data of the cable short sample. The load line ratio is calculated by dividing the design current by a maximum current. At the maximum current, the QC1RP and QC1LP can generate the maximum field gradient (G_{max}) of 105.6 T/m.

The superconducting cable is the Rutherford type, and it consists of 10 NbTi strands. The cable has a large key stone angle, 2.09 degrees, to position the cable at right angles to a circle inscribed on the inner surface of the coil. In the table, Cu/S ratio is the proportion of copper

Table 4
Magnet parameters of QC1RP/QC1LP.

Parameter	Value
Design field gradient, G_d	76.37 T/m
Design current, I_d	1800 A
Operation current, $I_{o(1RP,1LP)}$ @April 11,2020	1599 A, 1598 A
Peak field in coil winding at I_d, B_p	4.56 T
Load line ratio at I_d and 4.7 K, R_L	72.3%
Maximum field gradient at 4.7 K, G_{max}	105.6 T/m
Coil	
1st layer inner/outer radius, R_{i-c1}/R_{o-c1}	25.0 mm/27.65 mm
Coil length, L_{c1}	344.6 mm
Straight section length, L_{st-c1}	305.1 mm
Turns (1st, 2nd, 3rd coil block), T_{c1-1}, T_{c1-2}, T_{c1-3}	7, 3, 2
1st coil angle, θ_{c1-1}	0.272–16.57 deg.
2nd coil angle, θ_{c1-2}	18.50–25.49 deg.
3rd coil angle, θ_{c1-3}	29.00–33.66 deg.
2nd layer inner/outer radius, R_{i-c2}/R_{o-c2}	27.78/30.43 mm
Coil length, L_{c2}	361.9 mm
Straight section length, L_{st-c2}	301 mm
Turns (1st, 2nd, 3rd coil block) T_{c2-1}, T_{c2-2}, T_{c2-3}	8, 3, 2
1st coil angle, θ_{c2-1}	0.983–17.84 deg.
2nd coil angle, θ_{c2-2}	18.50–24.82 deg.
3rd coil angle, θ_{c2-3}	29.00–33.21 deg.
Collar inner/outer radius, R_{i-col}/R_{o-col}	30.75/35.5 mm
Physical magnet length, L_{pm}	409.3 mm
Effective magnetic length, L_{em}	333.6 mm
Stored energy at I_d, E_d	1.43 kJ
Inductance, L	0.88 mH
SC Rutherford cable (NbTi)	
Strand wire:	
Diameter, D_s	0.498 mm
Cu/S ratio	1.0
Filament diameter, D_f	7.7 μm
No. of filaments, N_f	2113
RRR of Cu	181
I_{c-b}/I_{c-a} bef./aft. cabling @ 5T, 4.22 K	326 A/317 A
@ 7T, 4.22 K	193 A/188 A
Cable:	
Width, W_c	2.50 mm
Middle thickness, T_{cm}	0.93 mm
Keystone angle, θ_k	2.09 deg.
No. of strands, N_s	10

Where B_p for the QC1P coil is the summation of the magnetic fields by QC1RP/LP and the solenoids.

to NbTi (superconducting material) in the strand wire. The cable cross section is shown in Fig. 6. The four coils are clamped with collars of YUS130S [13] to apply pre-stress of 30 MPa to the coils. The thickness of the collar is 4.75 mm. The number of turns of the 1st and 2nd coils are 12 and 13, respectively. For setting the magnets at the closest position to the IP, the coil ends are designed to be as short as possible, as shown in Fig. 5. The total length of both coil ends is 43.1 mm while the physical coil length is 361.9 mm. The corrector magnets are shown in the same figure, and the corrector wires are shown by the open circles. The magnets are a_1, b_1 and a_2 correctors starting from the innermost layer.

The calculated multipole field components of the 2D cross-section and the 3D integral coil configurations of the magnet are listed in Table 5. The multipole field components are designed to be within 1×10^{-4} (1 unit) at the reference radius, R_{ref}, of 10 mm for QC1RP and QC1LP. While field quality of the magnet is normally specified at two-thirds of the magnet aperture radius, R_{ref} of these quadrupole magnets are defined by the request of the beam optics group. Because R_{i-c1} of QC1RP and QC1LP is 25 mm, the ratio of R_{ref} to R_{i-c1} is 0.4. This smaller ratio than the usual case leads to the small higher multipole fields in the magnet design stage. In order not to generate skew field components in the coil lead end, where the cable ends exit in the coil, the design of the coil is mirror symmetric with respect to the neighbor coils in the four quadrant coils. The calculated error field components are b_6 of 0.10 units and b_{10} of −0.21 units by the 2D cross-section model, and b_4 of 0.24 units, b_6 of 0.54 units and b_{10} of −0.21 units

Table 5
Multipole field components of QC1LP/QC1RP @ R_{ref} = 10 mm.

Component	2D cross section, units	3D integral field, units
b_4	0	0.24
b_6	0.10	0.54
b_8	0	0.01
b_{10}	−0.21	−0.21
b_{12}	0.00	0.00
b_{14}	0.02	0.00

by the 3D full magnet model. The calculated field profiles along the magnet axis are shown in the section of "Magnetic field quality and alignment of the magnets".

For the colliding beam energy of 12 GeV the design magnet current is 1800 A. At present (as of November 4th, 2020), for 11 GeV colliding beam energy, the current for QC1RP and QC1LP is 1599.7 A and 1597.6 A, respectively. The load line ratios of these currents are about 64%.

The configuration of the beam pipe imposes a stringent limitation to this magnet design because the pipe is designed to be operated at room temperature. The outer radius of the beam pipe is 14.5 mm, and the inner radius of the cryostat inner pipe is 18 mm. The distance between two pipes at room temperature and at 4.5 K is 3.5 mm. As shown in Fig. 5, the beam pipe has a water-cooling channel, and the heat load at the pipe by the beam is removed by flowing water.

In Fig. 7, the QC1LP magnet, the four coils for the QC1RP magnet and the collars for QC1RP are shown.

(b) QC1RE and QC1LE quadrupole magnets

QC1LE and QC1RE [6] have magnetic yokes for reducing the leak magnetic field from the magnets to the e^+ beam line. The cross section and the SC coils of the magnet are shown in Fig. 8. The magnet parameters are listed in Table 6. The innermost and outermost radii of the SC coils are 33.0 mm and 38.425 mm. The design current of the magnets is 2000 A, and the field gradient is designed to be 91.57 T/m at the magnet center. The integral quadrupole field is 34.16 T and the effective magnetic length is 0.3731 m. The maximum field in the coil is 3.5 T at 2000 A, and the load line ratio at 4.7 K is 73.4%. The SC cable parameters are basically the same as that for QC1LP and QC1RP. The keystone angle has changed to 1.59 degree. In Table 7, the calculated multipole field components at R_{ref} of 15 mm for QC1RE and QC1LE with the 2D cross-section and the 3D integral coil configurations in the magnet are shown. The multipole field components are designed to be within 1 unit. The error field components are b_6 of −0.05 units and b_{10} of −0.26 units with the 2D cross-section model, and b_4 of −0.01 units, b_6 of −0.03 units and b_{10} of −0.33 units with the 3D full magnet model.

While the magnets are operated in the Belle solenoid field at 1.5 T with the ESR1 and ESL solenoids, the solenoid field along QC1RE and QC1LE is reduced to almost zero. However, the actual Belle solenoid field is not perfectly and locally canceled with ESR1 and ESL. The uncanceled field is absorbed into the magnetic yokes. Together with the magnetic field induced by QC1LE or QC1RE it easily saturates the yokes. At the IP side of the magnets, where the magnets and the e^+ beam line are closest, the space for an iron is not sufficient. To avoid this saturation, Permendur [14] was chosen instead of iron as the yoke material. It has a saturated magnetic flux density of 2.30 T.

The effect of Permendur was studied with the calculation model as shown in Fig. 9, which shows the cross section on the IP side of the magnet-cryostat. To fit within the allocated space between the e^+ beam pipe and the inner bore of the LHe vessel in the cross section, the outer perimeter of the yoke was pruned away. For evaluating the leak field from QC1RE to the e^+ beam line, the magnetic field in the cross section was calculated. The results are shown in Table 8. The magnet current is 1577 A, and it corresponds to beam operation at the colliding energy of 11 GeV. For the case of iron for the yoke and magnetic shield with no solenoid field, the leak field from QC1RE was 1.52×10^{-4} T at the center of the e^+ beam pipe. With Permendur, the leak field was reduced to 1.4×10^{-5} T. If the magnetic field due to the solenoids in the yoke and the shield is increased to 1 T, the leak field for iron was calculated to be 1.39×10^{-3} T while the field for Permendur was 8.2×10^{-5} T. The leak field with iron is not acceptable for the beam operation. When the accelerator is operated at the colliding energy of 12 GeV, and the magnet current would be increased to 1971.3 A. In this operation, the leak field at the field of 1 T in the iron yoke and the shield reaches to 3.05×10^{-3} T, and the field with Permendur is still low and 1.56×10^{-4} T. Permendur was thus evaluated to give excellent magnetic performance for the system.

Table 6
Magnet parameters of QC1RE and QC1LE.

Parameter	Value
G_d	91.57 T/m
I_d	2,000 A
$I_{p(1RE,1LE)}$ @April 11,2020	1498.6 A, 1581.0 A
B_p at I_d	3.50 T
R_L at I_d and 4.7 K	73.4%
G_{max}	125.8 T/m
Coil	
1st layer R_{i-c1}/R_{o-c1}	33.0 mm/35.65 mm
L_{c1}	401.1 mm
L_{st-c1}	330.0 mm
T_{c1-1}, T_{c1-2}, T_{c1-3}	9, 5, 2
θ_{c1-1}	0.125–16.20 deg.
θ_{c1-2}	17.70–26.63 deg.
θ_{c1-3}	32.50–36.07 deg.
2nd layer R_{i-c2}/R_{o-c2}	35.78 mm/38.43 mm
L_{c2}	396.6 mm
L_{st-c2}	338.3 mm
T_{c2-1}, T_{c2-2}, T_{c2-3}	10, 5, 3
θ_{c2-1}	0.116–16.64 deg.
θ_{c2-2}	17.70–25.96 deg.
θ_{c2-3}	31.58–36.54 deg.
R_{i-col}/R_{o-col}	38.75 mm/47.0 mm
Yoke inner/outer radius, R_{i-y}/R_{o-y}	47.0 mm/70.0 mm
L_{pm}	455.4 mm
L_{em}	373.1 mm
E_d	4.38 kJ
L	2.19 mH
SC Rutherford cable (NbTi)	
Strand wire: same design as QC1P	
D_f	7.6 μm
RRR of Cu	186
I_{c-b}/I_{c-a} @ 5T, 4.22 K	328 A/307 A
@ 7T, 4.22 K	194 A/183 A
Cable: θ_k	1.59 deg.

Table 7
Multipole field components of QC1LE/QC1RE @ R_{ref} = 15 mm.

Component	2D cross section, units	3D integral field, units
b_4	0	−0.01
b_6	−0.05	−0.03
b_8	0	0.04
b_{10}	−0.26	−0.33
b_{12}	0	0.04
b_{14}	−0.01	−0.06

Table 8
Leak field of QC1LE/QC1RE to e^+ beam line.

Current, A	Field in yoke, T	Iron, T	Permendur, T
1577	0	1.52×10^{-4}	1.4×10^{-5}
	0.5	1.75×10^{-4}	1.9×10^{-5}
	1.0	1.39×10^{-3}	8.2×10^{-5}
1971.3	0	2.47×10^{-4}	1.9×10^{-5}
	0.5	3.53×10^{-4}	3.4×10^{-5}
	1.0	3.05×10^{-3}	1.56×10^{-4}

(c) QC2RP and QC2LP quadrupole magnets

QC2RP and QC2LP magnets [7] are positioned behind QC1RP and QC1LP from the IP, as shown in Fig. 1. The cross-section and the SC

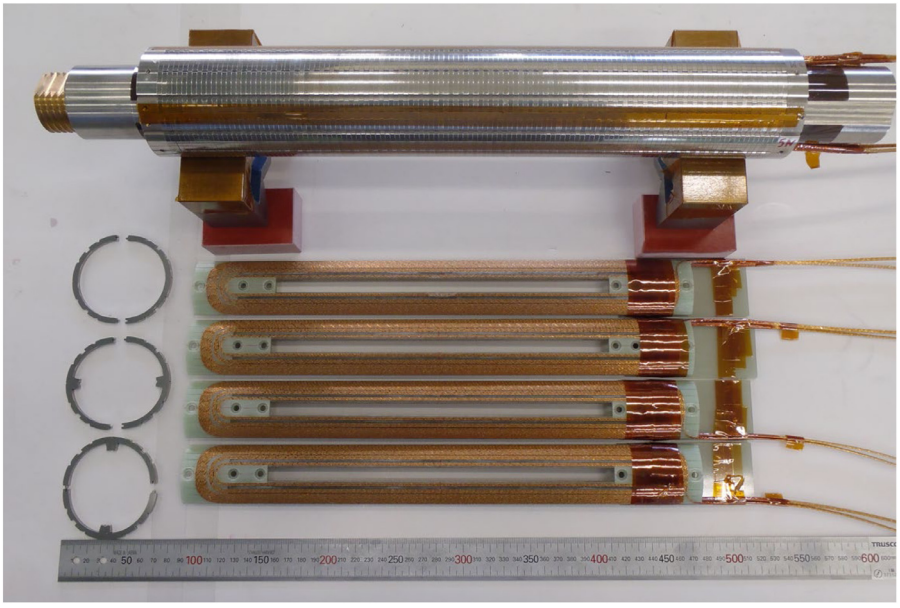

Fig. 7. QC1LP magnet, four superconducting coils for QC1RP and YUS130S collars (in the left side of the picture).

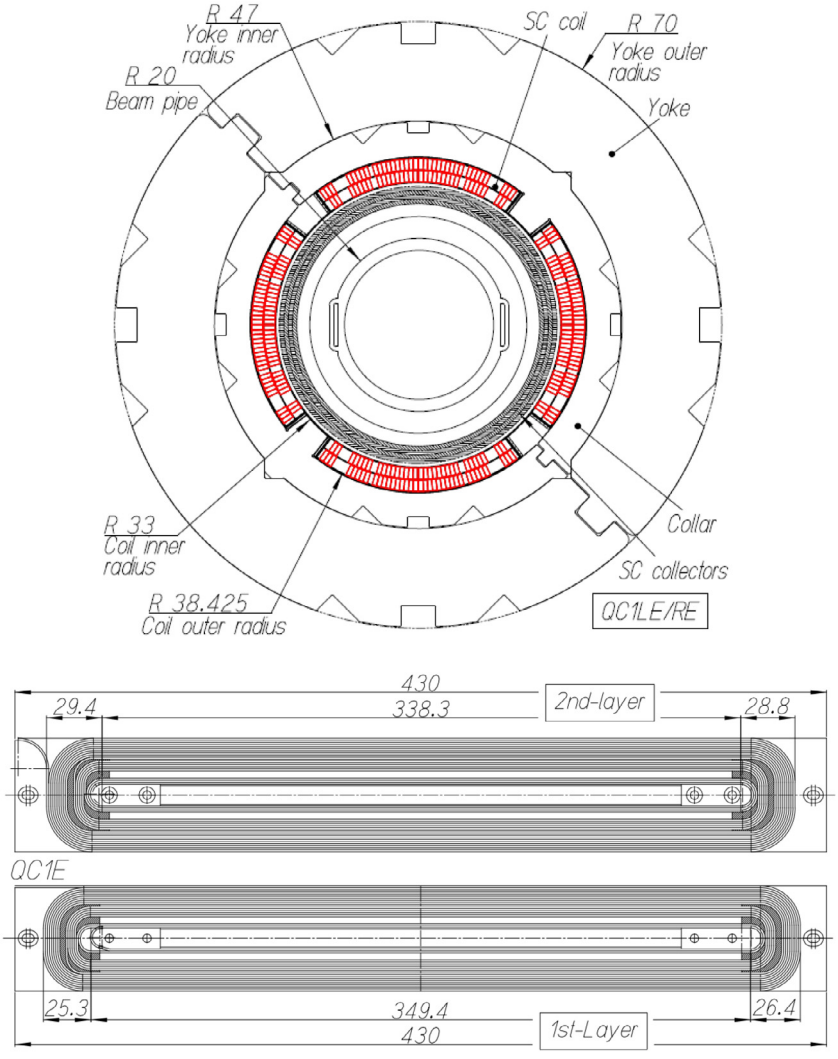

Fig. 8. Cross section and coil design of QC1RE and QC1LE.

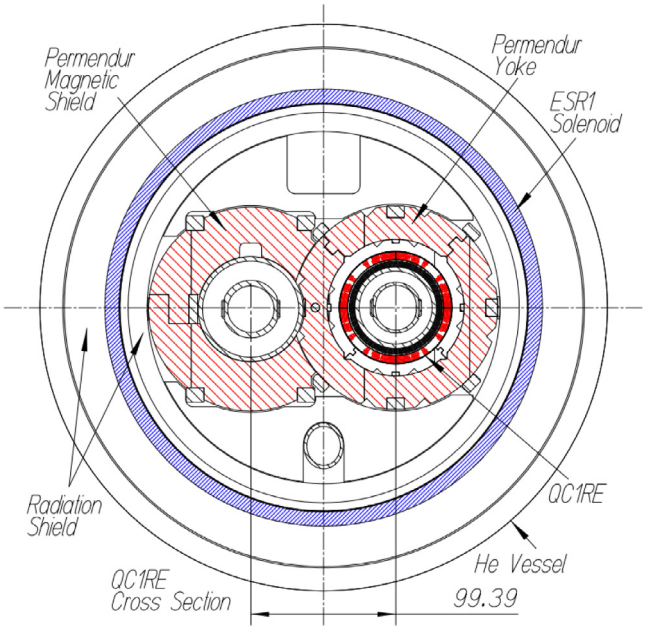

Fig. 9. Cross section of the QC1RE cold mass in the IP side.

coils of the QC2RP and QC2LP are shown in Fig. 10. The magnet design concept is the same as the QC1RE and QC1LE.

The design current and the field gradient of this magnet are 1000 A and 31.97 T/m, and the load line ratio is 44% at 4.7 K. The material of the magnetic yoke is Permendur because of the reduction of the leak field from the magnets to the HER beam line. The magnet parameters are shown in Table 9. The SC cable parameters are same as the QC1P and QC1E magnets except that the cable key stone angle is 1.00 degree.

The calculated multipole field components at R_{ref} of 30 mm with the 2D magnet cross-section and the 3D integral magnet configuration are listed in Table 10. The error field components are b_6 of −0.003 units and b_{10} of −0.10 units with the 2D magnet cross-section model, and b_4 of −0.04 units, b_6 of 0.18 units and b_{10} of −0.96 units with the 3D magnet model.

(d) QC2RE and QC2LE quadrupole magnets

The cross-sections and the SC coils of QC2RE and QC2LE [7] are shown in Fig. 11. While the two magnets have the same SC coil cross section design, the designs of the assembled magnet unit are quite different. In the QCS-R cryostat, the ESR2 and ESR3 solenoids are set on the e^- and e^+ beam lines, respectively. Because of the tight space constraint in the cryostat, ESR2 is incorporated in the area between the coil collars and the iron yokes of QC2RE. Therefore, the inner radii of the yokes of QC2RE and QC2LE are different. QC2RE has four SC corrector magnets inside the SC quadrupole coils. As a result, the assembled magnets are extremely complicated devices.

The magnet parameters are listed in Table 11. The innermost and outermost radii of the SC coils are 59.30 mm and 64.725 mm. The design currents of QC2RE and QC2LE are 1562.5 A and 1250 A, and the field gradients are designed to be 38.56 T/m and 36.39 T/m, respectively. The integral quadrupole fields of are 16.16 T and 19.54 T with the effective magnetic lengths of 0.419 m and 0.537 m, respectively.

The calculated multipole field components at R_{ref} of 35 mm for QC2RE and QC2LE are listed in Table 12. In the 2D cross section model, the error field components are b_6 of −0.19 units and −0.16 units, and b_{10} of −0.11 units and −0.09 units for QC2RE and QC2LE, respectively. In the 3D model, b_{10} of QC2RE and QC2LE are more than 1 unit, and they are −1.88 units and −1.30 units, respectively.

Table 9
Magnet parameters of QC2RP and QC2LP.

Parameter	Value
G_d	31.97 T/m
I_d	1,000 A
$I_{o(2RP,2LP)}$ @April 11,2020	882.4 A, 878.5 A
B_p at I_d	2.43 T
R_L at I_d and 4.7 K	44%
G_{max}	72.7 T/m
Coil	
1st layer R_{i-c1}/R_{o-c1}	53.8 mm/56.45 mm
L_{c1}	442.3 mm
L_{st-c1}	370.0 mm
T_{c1-1}, T_{c1-2}	19, 7
θ_{c1-1}	0.078–21.21 deg.
θ_{c1-2}	26.30–34.08 deg.
2nd layer R_{i-c2}/R_{o-c2}	56.58 mm/59.23 mm
L_{c2}	443.6 mm
L_{st-c2}	369.0 mm
T_{c2-1}, T_{c2-2}	20, 7
θ_{c2-1}	0.247–21.41 deg.
θ_{c2-2}	25.20–32.61 deg.
R_{i-col}/R_{o-col}	59.6 mm/68.0 mm
R_{i-y}/R_{o-y}	68.0 mm/93.0 mm
L_{pm}	495.5 mm
L_{em}	409.9 mm
E_d	3.66 kJ
L	7.32 mH
SC Rutherford cable (NbTi)	
Strand wire: same design as QC1P	
D_f	7.7 μm
RRR of Cu	178
I_{c-b}/I_{c-a} @ 5T, 4.22 K	326 A/309 A
@ 7T, 4.22 K	193 A/185 A
Cable: θ_k	1.00 deg.

Table 10
Multipole field components of QC2RP/QC2LP @ R_{ref} = 30 mm.

Component	2D cross section, units	3D integral field, units
b_4	0	−0.04
b_6	−0.003	0.18
b_8	0	0.08
b_{10}	−0.10	−0.96
b_{12}	0	0.02
b_{14}	−0.03	−0.07

3.4. Compensation solenoids

ESL and ESR1/2/3 solenoids cancel the integral Belle II solenoid field in the left and right side from the IP, respectively. The IP position shifts by 0.47 m to the left side along the solenoid axis with respect to the Belle II detector center as shown in Fig. 2, and in consequence, the integral solenoid field in each side is different. The integral solenoid fields from the IP to be canceled are 2.31 Tm and 3.86 Tm for the left and right side, respectively.

(a) ESL and ESR1

Fig. 12 shows the horizontal cross section of the QCS-L cryostat and the ESL coils. The ESL is in front of the LHe vessel. ESL is composed of 12 short solenoid coils to generate the designed field profile. From the 1st coil, which is the closest one to the IP, to the 7th coil, QC1LP is installed at the inner side of the solenoid bore. There is no magnetic material in this region. From the 8th coil to the 12th coil, QC1LE and QC2LP with the Permendur yokes and the magnetic shield on the beam lines are assembled in these solenoid bores. The 7th to 12th coils are designed to cancel the Belle II solenoid field of 1.5 T along the solenoid axis so that the QC1LE magnetic yoke and the magnetic shield are not saturated magnetically. The solenoid fields on the two beam lines from the 7th to 12th coils are quite close to zero because of the good magnetic performance of Permendur. The 1st to 6th coils cancel the integral Belle II solenoid field from the IP. Since QC1LP is a collared-magnet without a yoke, the solenoid field profiles in the beam lines

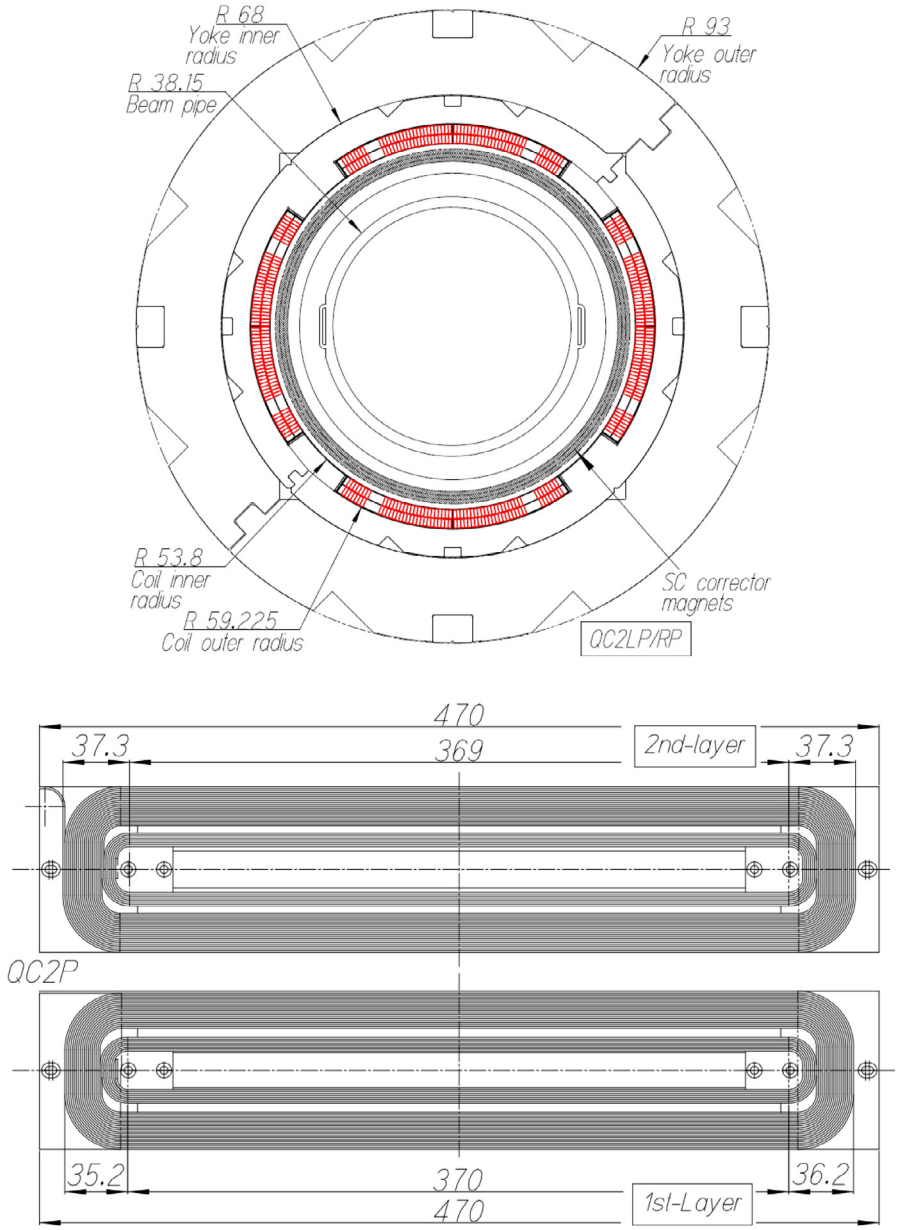

Fig. 10. Cross section and coil design of QC2RP and QC2LP.

can be calculated by summation of the solenoid fields of the Belle II solenoid and the ESL. The completed ESL solenoid in the factory is shown in Fig. 13.

Fig. 14 shows the cross section of the QCS-R cryostat. ESR1 is composed of 15 short solenoid coils. Based on the same magnetic design as QCS-L, ESR1 encloses QC1RP, QC1RE and QC2RP. The Belle II solenoid field from IP is integrally canceled with the 1st to 7th coils, and the 8th to 15th coils cancel locally the Belle II solenoid field.

The magnet parameters of ESL and ESR1 are shown in Table 13. The magnet length and the coil turns of ESL and ESR1 are 914 mm and 4610, and 1575 mm and 6237, respectively. The operation current and the peak magnetic field in the coil for ESL and ESR1 are 390 A and 3.56 T, and 450 A and 3.05 T, respectively. The load line ratios of R_L are smaller than 50% for both. The geometries of the small coils and their turn number (T_{num-c}) are shown in the table. The SC cable is the rectangle NbTi wire, and the size is 0.93 mm in height and 1.380 mm in width. The critical current at 4.22 K and 4 T is 1814 A.

Due to the magnetic components in the solenoid bores, the inductances (L) of ESL and ESR1 change with the transport current to the solenoids. The change of L with the current by calculation and measurement is shown in Fig. 15. At 0 A of ESL and ESR1, the magnetic components in the solenoid bores are in a complete magnetic saturation condition due to the Belle II solenoid field. In this case, L of ESL and ESR1 are 1.16 H and 1.69 H by calculation, respectively. By increasing the ESL and ESR1 currents, the magnetic components return to the unsaturated state, and L of ESL and ESR1 at I_d increased to 2.46 H and 8.04 H by calculation, respectively. The changes of L were measured, and the data are shown in the same figure.

To adjust the integral solenoid fields along the beam lines during the beam operation, an additional current lead is attached to the SC coil cable in the transition between the 6th and 7th coils for ESL and ESR1, respectively.

The solenoid field profiles of the axial direction, B_z, and the radial direction, B_r, along both beam lines are shown in Fig. 16. The position of $Z = 0$ in the figure is the IP, and the red and blue lines correspond to the field components on the HER and LER beam lines, respectively. On the Z axis, the plus and minus values are the positions in the right and

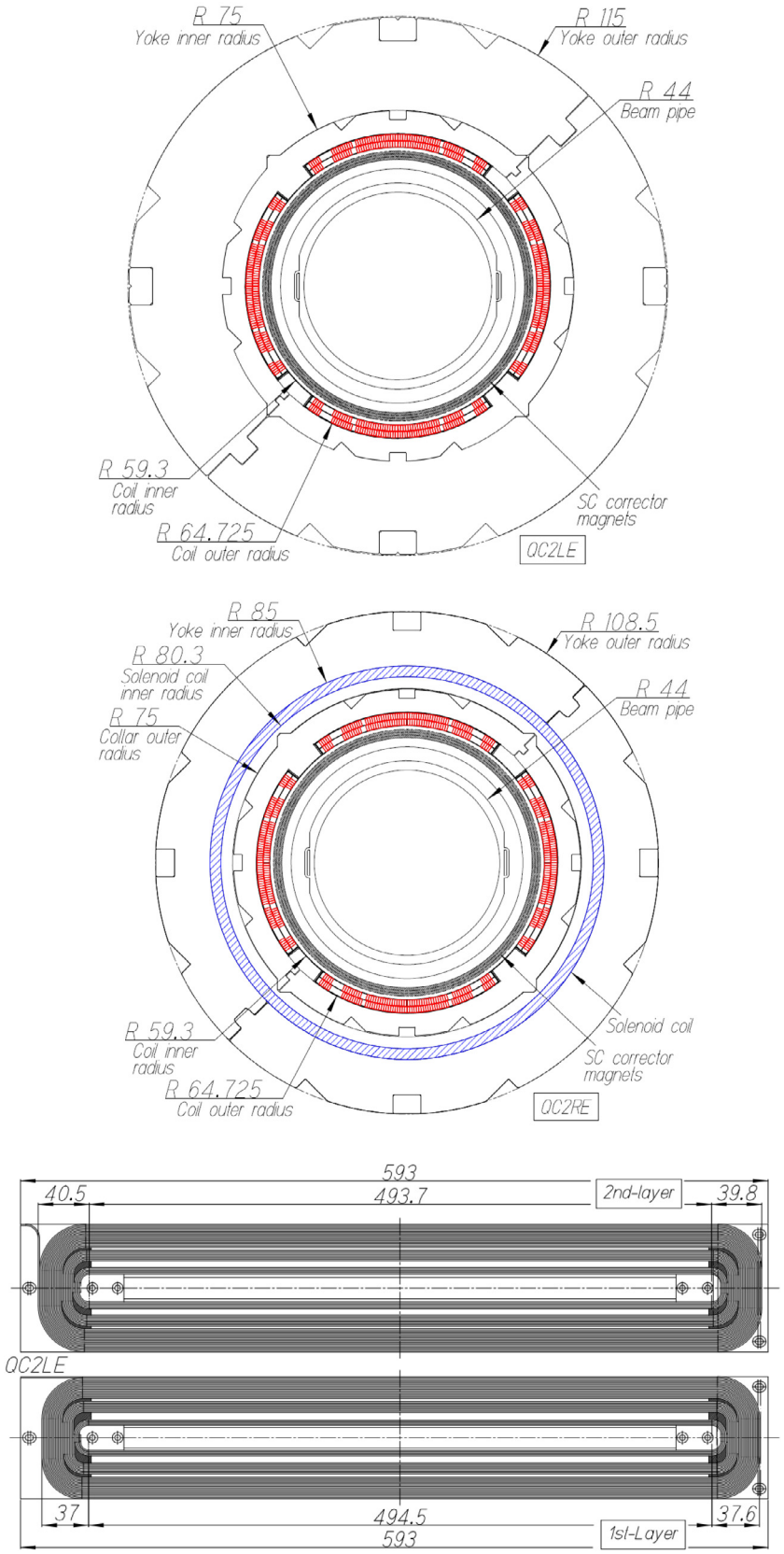

Fig. 11. Cross sections of QC2LE and QC2RE, and coil design of QC2LE.

left sides, respectively. While the B_z profiles along the two beams are almost coincident, the B_r components are of opposite sign with respect to each other due to the beam crossing angle of 83 mrad.

On the left side from the IP, the solenoid field from Belle II is canceled with the 1st to the 7th coils of ESL. For canceling the integral Belle II solenoid field, ESL is designed to generate a higher field than

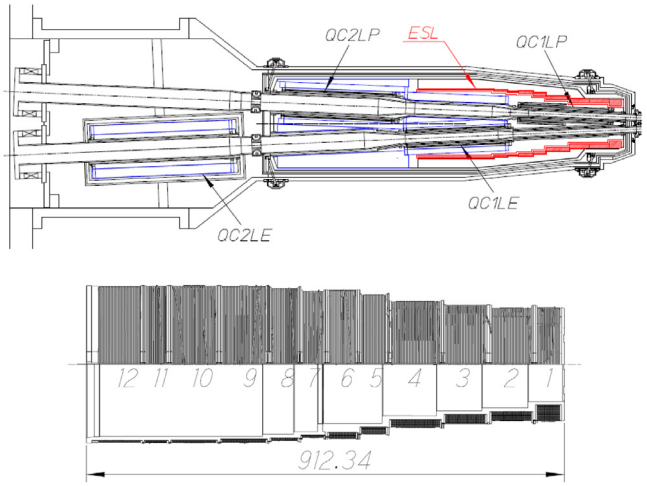

Fig. 12. Horizontal cross section of QCS-L cryostat, and the external and cross section view of ESL solenoid.

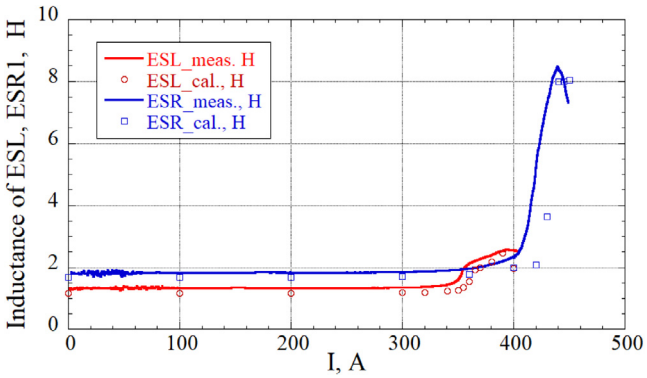

Fig. 15. Inductance of ESL and ESR1 as a function of solenoid current. Solid lines are measurement data, and symbols are calculation data.

1.5 T, oppositely signed, due to the shorter coil length compared to the Belle II field area. Therefore, the peak of the combined field reaches −2.36 T. In the area of −2<z<-1.3, the solenoid field is reduced to almost zero by the cancellation with ESL, the Permendur magnet yoke, and the magnetic shield components. As a consequence, the solenoid field on the beam lines in the area is reduced to less than 1 Gauss.

In the right side for 0 <z< 2, the combined solenoid field profile is almost mirror symmetrical with respect to the left side, and the peak

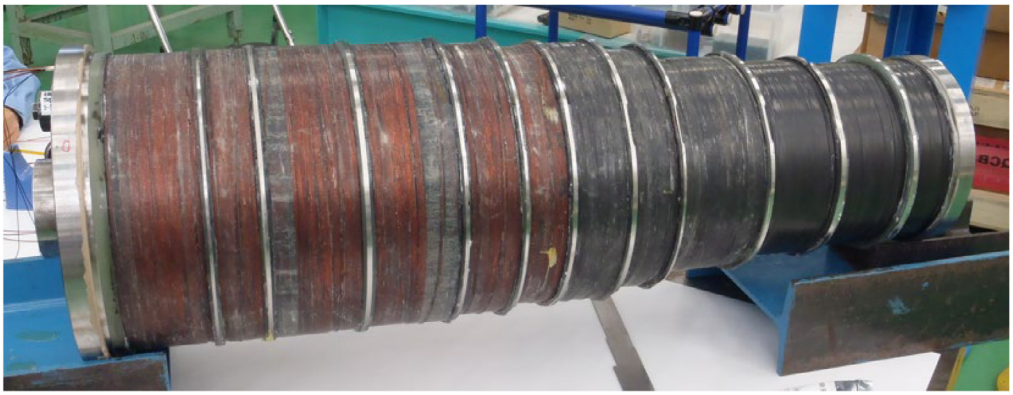

Fig. 13. Completed ESL solenoid.

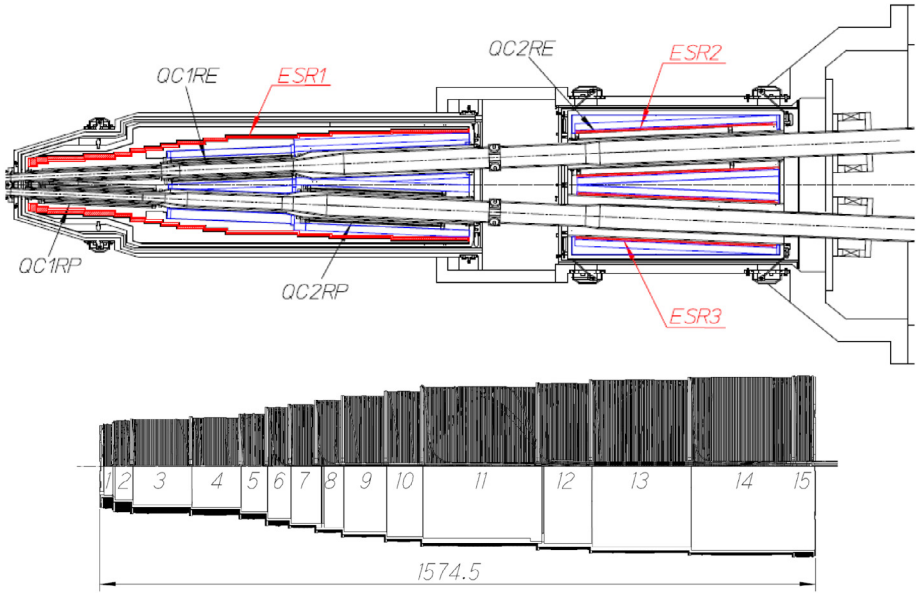

Fig. 14. Horizontal cross section of QCS-R cryostat, and the external and cross section view of ESR1 solenoid.

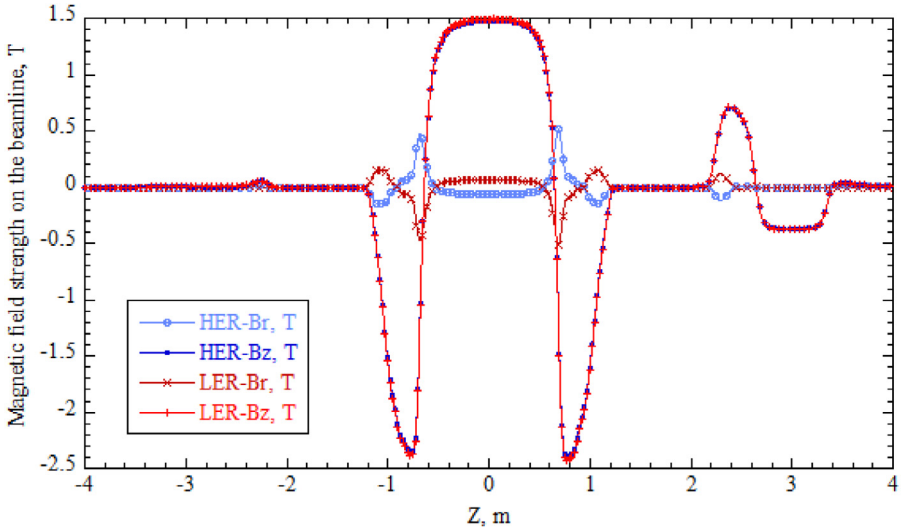

Fig. 16. Magnetic field profiles along the beam lines.

Table 11
Magnet parameters of QC2RE and QC2LE.

Parameter	
$G_{d(2RE,2LE)}$	38.56 T/m, 36.39 T/m
$I_{d(2RE,2LE)}$	1562.5 A, 1,250 A
$I_{o(2RE,2LE)}$ @April 11,2020	1249.2 A, 1001.1 A
$B_{p(2RE,2LE)}$ at I_d	2.81 T, 2.63 T
$R_{L\ (2RE,2LE)}$ at I_d and 4.7 K	57.4%, 50.0%
$G_{max(2RE,2LE)}$	67.2 T/m, 72.8 T/m
Coil	
1st layer R_{i-c1}/R_{o-c1}	59.3 mm/61.95 mm
$L_{c1(2RE,2LE)}$	451.1 mm, 569.1 mm
$L_{st-c1(2RE,2LE)}$	376.5 mm, 494.5 mm
T_{c1-1}, T_{c1-2}, T_{c1-3}	16, 8, 4
θ_{c1-1}	0.071–16.25 deg.
θ_{c1-2}	18.3–26.39 deg.
θ_{c1-3}	31.8–35.85 deg.
2nd layer R_{i-c2}/R_{o-c2}	62.08 mm/64.73 mm
$L_{c2(2RE,2LE)}$	455.9 mm, 573.9 mm
$L_{st-c2(2RE,2LE)}$	375.7 mm, 493.7 mm
T_{c2-1}, T_{c2-2}, T_{c2-3}	17, 8, 5
θ_{c2-1}	0.068–16.51 deg.
θ_{c2-2}	18.25–25.99 deg.
θ_{c2-3}	30.45–35.28 deg.
R_{i-col}/R_{o-col}	65.05 mm/75.0 mm
$R_{i-y}/R_{o-y(2RE,2LE)}$	85 mm/108.5 mm, 75.0 mm/115.0 mm
$L_{pm(2RE,2LE)}$	560.7 mm, 618.9 mm
$L_{em(2RE,2LE)}$	419.0 mm, 537.0 mm
$E_{d(2RE,2LE)}$	12.61 kJ, 10.38 kJ
$L_{(2RE,2LE)}$	10.36 mH, 13.28 mH
SC Rutherford cable (NbTi)	
Strand wire: same design as QC1P	
D_f, μm	7.7
RRR of Cu	183
I_{c-b}/I_{c-a} @ 5T, 4.22 K	326 A/313 A
@ 7T, 4.22 K	193 A/186 A
Cable: θ_k	0.94 deg.

Where B_p for the QC2RE coil is the summation of the magnetic fields by QC2RE and ESR2.

field is −2.40 T. In the region of 2 <z< 2.6, there exists a positive field bump of B_z on each beamline. This bump is due to the Belle II solenoid field in the space without a magnetic shield between two LHe vessels in the QCSR cryostat. This solenoid field is canceled with ESR2/3 for HER and LER, respectively. The integral solenoid fields with and without ESL and ESR1/2/3 are shown in Table 14. The canceled integral solenoid fields on the beam lines from the IP to ± 4 m are less than 1% of the integral Belle II solenoid field. They were adjusted to zero after the magnetic field measurements.

Table 12
Multipole field components of QC2RE/QC2LE @ R_{ref} = 35 mm.

Comp.	2D QC2RE/QC2LE, units		3D QC2RE/QC2LE, units	
b_4	0	0	0.07	0.05
b_6	−0.19	−0.16	−0.04	−0.09
b_8	0	0	0.06	0.04
b_{10}	−0.11	−0.09	−1.88	−1.30
b_{12}	0	0	0.03	0.02
b_{14}	0.03	0.02	−0.05	−0.03

Table 13
Magnet parameters of ESL and ESR1.

Parameter	ESL	ESR1
L_{pm}	914 mm	1575 mm
T_{num-s}	4610	6237
I_d	390 A	450 A
B_p at I_d	3.56 T	3.05 T
L at I_d	2.46 H	8.04 H
E_d	187 kJ	814 kJ
R_L at 4.7 K	49.9%	46.4%
R_{i-c} /R_{o-c}/Lc, mm, T_{num-c}		
#1	78/109/44, 744	70/93/20, 273.8
#2	91/108/76, 715	79/101/34, 435
#3	96/113/76, 735	91/103/124, 963
#4	106/121/93, 768	95/107/102, 700
#5	120/133/47, 325	105/116/52, 307
#6	130/142/51, 329	120/131/44, 268
#7	136/140/40, 88	130/136/52, 164
#8	141/145/50, 126	140/146/52, 154
#9	143/150/84, 281	150/156/89, 238
#10	145/151/84, 242	160/166/73, 210
#11	145/150/40, 102	170/176/249, 716
#12	145/149/81, 155	178/183/110, 326
#13	NA	185/191/211, 594
#14	NA	190/196/223, 671
#15	NA	189/199/38, 217
SC cable (NbTi)	Rectangular wire	
Cable size	0.93 mm ×1.380 mm 1.03 mm ×1.480 mm (with insulation)	
D_f	19 μm	
N_f	1500	
Cu/S ratio	1.8	
RRR of Cu	171	
I_c @ 4T, 4.22 K	1814 A	
@ 6T, 4.22 K	1149 A	

T_{num-S} and T_{num-c} are the total turn number of the solenoid and the turn number of each short solenoid coil, respectively.

Table 14
Integral solenoid field.

	−4< z < 0, Tm		0 < z < 4, Tm	
	LER	HER	LER	HER
Without ESL, ESR1/2/3	2.31	2.31	3.86	3.86
With ESL, ESR1/2/3	0.022	0.021	0.024	0.024

Table 15
Magnet parameters of ESR2 and ESR3.

Parameter	ESR2/3
L_{pm}	720 mm
T	1356
I_d	151.1 A
R_{i-c} /R_{o-c}/Lc	81.1 mm/84.3 mm/683 mm
B_p at I_d	0.3 T
L at I_d	0.0635 H
E_d	0.725 kJ
R_L at 4.7 K	11%

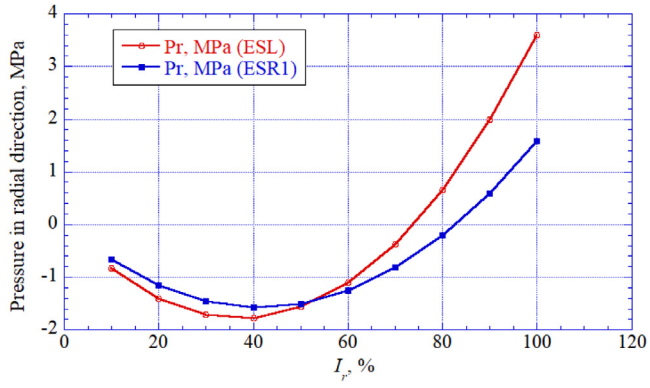

Fig. 17. Pressure by the electro-magnetic force on the ESL and ESR1 support bobbin. I_r is the ratio of the transport current to the design currents of ESL and ESR1.

(b) ESR2 and ESR3

ESR2 and ESR3 are set on each beam line in the LHe vessel furthest from the IP in the QCS-R cryostat. The two solenoids are constructed with the same magnet parameters, and the integral fields are 0.17 Tm. The magnet parameters are shown in Table 15. The SC cable is same as the cable for ESL and ESR1. ESR2 and ESR3 are connected in series, and they are excited with one power supply. ESR2 is installed between the QC2RE collars and the yokes as already shown in Fig. 11, and ESR3 is set on the LER beam line within the magnetic shield.

(c) Electromagnetic force on the compensation solenoids

ESL, ESR1 and ESR2/3 generate the solenoid fields in the opposite direction with respect to the Belle II solenoid field. As the result, these solenoids experience large electro-magnetic forces (EMF) due to interaction with the Belle II solenoid field. The EMF in the coil axial direction act on the ESL and ESR1 with 52.6 kN and 33.7 kN at the design currents, respectively, and the coils are pushed outward from the IP when the solenoid magnets are excited. The position changes of the SC magnets due to the EMFs are reported in the section of "Magnetic field quality and alignment of the magnets". The support system of the magnet assembly against the electro-magnetic forces is explained in the section of "Cryostat mechanical design".

As for the EMF in the radial direction on the coil winding, in general, a solenoid coil has an outward-directed EMF. In case of these compensation solenoids, the inward-directed forces act on the coil by interaction with the Belle II solenoid field. The EMF in the radial direction on the #1 coils in ESL and ESR1 produces the pressure on the solenoid bobbin. The pressure is shown as a function of the ratio of the transport current to the design current, I_r, in Fig. 17. For the transport currents less than 73% and 82% of I_r for ESL and ESR1, respectively,

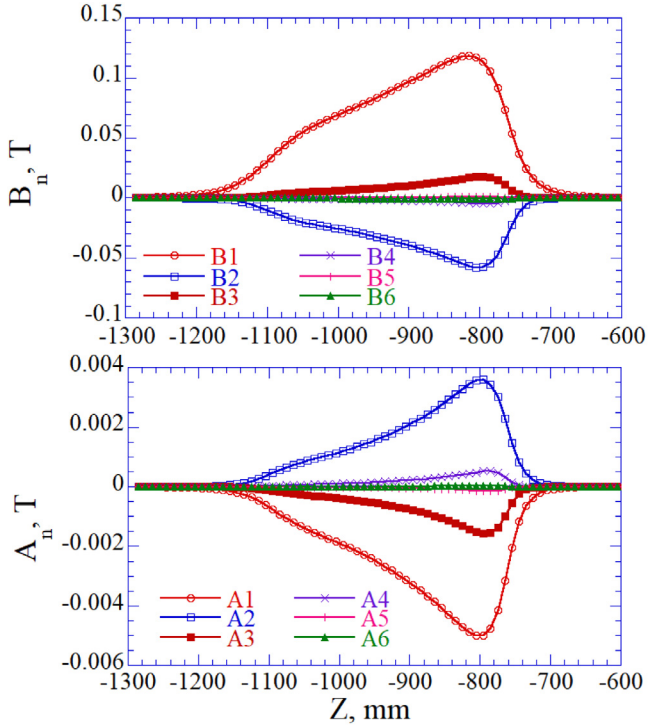

Fig. 18. QC1LP leak field profiles along HER beam line.

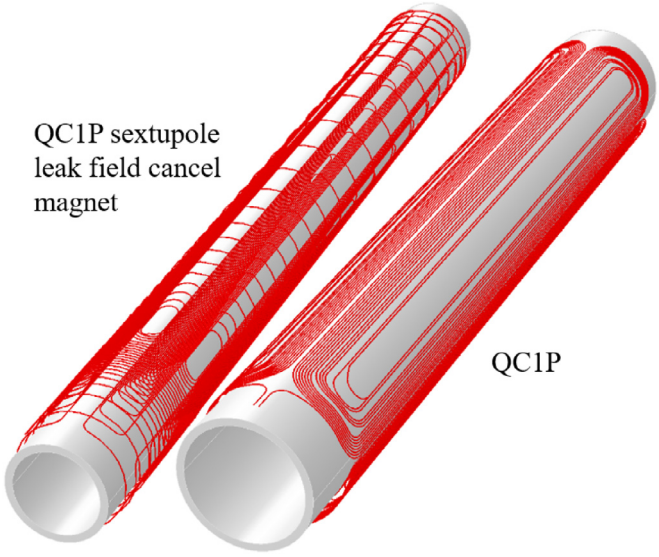

Fig. 19. Line current model of the QC1P quadrupole magnet and QC1L sextupole leak field cancel magnet on the beam lines.

the EMFs in the radial direction are directed inward and act on the solenoid bobbins. From the calculation result, the thickness of the coil bobbin was designed to withstand these forces.

3.5. Corrector magnets

The 35 corrector magnets were constructed by the BNL direct-wind method [15] under the U.S.-Japan Science and Technology Cooperation Program in High Energy Physics. They are assembled in two cryostats with the main quadrupole magnets and the compensation solenoids. The different shapes of the magnets were designed based on a multi-layer coil structure, using NbTi wire of ϕ 0.35 mm. Each main

Table 16
Integral field of corrector magnets.

	Type	QCSL			QCSR		
		Optics spec.	Design 60 A	Δ	Optics spec.	Design 60 A	Δ
QC1LP QC1RP	a_1	0.016	0.0181	0.7	0.016	0.0177	0.6
	b_1	0.016	0.0158	0.6	0.016	0.0161	0.5
	a_2	0.64	0.843	18	0.64	0.814	17
	b_4	60	304	–	60	283	–
	$a_3^{\#}$	–	–	–	5.1	9.18	–
QC2LP QC2RP	a_1	0.03	0.0358	1.2	0.03	0.0580	4.0
	b_1	0.03	0.0411	2.3	0.03	0.0426	1.3
	a_2	0.31	0.672	28	0.31	0.637	27
	b_4	60	164	–	–	–	–
	a_3	–	–	–	0.905	1.54	–
QC1LE QC1RE	a_1	0.027	0.0326	0.9	0.027	0.0319	1.0
	b_1	0.046	0.0561	0.9	0.046	0.0554	0.9
	a_2	0.75	0.976	17	0.75	0.912	17
	b_4	60	817	–	–	–	–
	a_3	–	–	–	4.55	22.1	–
QC2LE QC2RE	a_1	0.015	0.0411	2.5	0.015	0.0314	2.3
	b_1	0.015	0.0447	2.9	0.015	0.0368	2.7
	a_2	0.37	0.769	25	0.37	0.623	23
	b_4	60	146	–	–	–	–
	a_3	–	–	–	1.05	6.47	–
QC12RE	b_3	–	–	–	18.2	45.2	–
QC12RP	b_3	–	–	–	11.5	23.2	–

a_3 corrector magnet was designed for QC1RP, but this corrector magnet was misassembled with rotation angle of 90 degree in KEK. In the real system, the magnet works as the b_3 corrector as shown in Table 1. In the table, the unit of the integral field is Tm for a_1 and b_1, T for a_2, T/m for a_3 and b_3 and T/m^2 for b_4. The unit for Δ is mm for a_1 and b_1, mrad for a_2.

quadrupole magnet has the a_1, b_1 and a_2 corrector magnets inside of the magnet bore for adjusting the alignment of the magnetic center and the quadrupole field angle. The a_3 and b_3 corrector magnets are assembled in the QCS-R cryostat in order to reduce the effect of the sextupole field induced by fabrication errors of the SC quadrupole magnets [16]. The b_4 corrector magnets are used for tuning the dynamic aperture. The 30 corrector magnets are assembled inside the quadrupole magnet bores. The b_4 of QC1LP and the b_4 and $a_3(b_3)$ corrector for QC1RP are assembled on the periphery of the magnet collar. The a_3 corrector magnet for QC1RP was misassembled in KEK, consequently, this corrector magnet works as b_3. Two b_3 corrector magnets are installed between QC1 and QC2 for two beam lines in the QCS-R cryostat.

The required integral fields from the beam optics and the calculated integral field at 60 A of the correctors are listed in Table 16. As to the a_1, b_1 and a_2 corrector magnets, the possible alignment values of the quadrupole centers or the field angle are shown as Δ in the table. The a_1 and b_1 magnets were designed to correct the misaligned shift of the magnetic center in the vertical and horizontal directions, respectively. As shown in Table 16, for QC1LP, the center shift of the quadrupole field up to ±0.7 mm vertically and ±0.6 mm horizontally can be corrected with the a_1 and b_1 magnets, respectively. The a_2 magnet can correct the roll angle up to ±18 mrad. All corrector magnets are individually excited with the bipolar power converters. The magnet and the SC wire parameters are shown in Tables 17 and 18, respectively. The load line ratios at 60 A of the magnets are smaller than 38% at 4.7 K.

3.6. QC1P leak field cancel magnets

The QC1LP and QC1RP quadrupole magnets are collared magnets built without magnetic yokes. In this magnetic design scheme, the stray fields from these magnets leak into the adjacent beam line (HER). The calculated leak field profiles of QC1LP are shown in Fig. 18. The effect of these leak fields on the beam optics was studied. As the result, the dipole and quadrupole field components are included in the beam optics and the sextupole, octupole, decapole and dodecapole field components are canceled using special magnets [9,17].

The axial field profile of each leak field component varies significantly along the HER beam line because of the crossing angle between the HER and LER beam lines and the vertical offset of 1.5 mm for QCS-L and 1.0 mm for QCS-R, respectively.

In Fig. 19, the 3D line current models of the QC1LP magnet and the sextupole leak field cancel magnets are shown. And in Fig. 20, a view of the coils projected on a flat plane is shown. The midplane of the leaking sextupole field is twisted because the two beam lines have offset axes and a crossing angle of 83 mrad. The leak field cancel magnets are designed to cancel the normal and skew field components. The four types of magnets in each side of IP are assembled in a multi-layering configuration. They are connected to individual power converters. The operation current was decided by magnetic field measurements on the beam lines. In Table 19, the leak field cancel magnet parameters are listed. The SC wire parameters for the magnets are the same as the corrector magnets. In Fig. 21, the coil production of the QC1LP octupole leak field cancel magnet with the direct winding method in BNL is shown.

As the clear viewable description of this complicate superconducting device, the assembled condition of the QC1LP, QC1LE and QC2LP magnets, the corrector magnets and the QC1LP leak field cancel magnets in the stainless-steel support block is shown in Fig. 22. This completely assembled block is inserted into the bore of the ESL solenoid.

4. Magnetic field quality and alignment of the magnets

The magnetic field performance of all superconducting magnets was measured and confirmed at room temperature and at 4 K during the construction processes. In this paper, only the results of the magnetic field measurements after installing the magnet-cryostats in the beam lines are shown. The field measurements on the quadrupole and corrector magnets, the solenoids and the magnet alignment were performed with the harmonic coil system [18,19], the Hall probe [20] and the single stretched wire (SSW) [21–23], respectively.

4.1. Field performance measurements of QC1, QC2 and correctors

(a) Harmonic coil measurement system

The harmonic coil probe was composed of two harmonic coils, which are different in length for the integral field measurement and

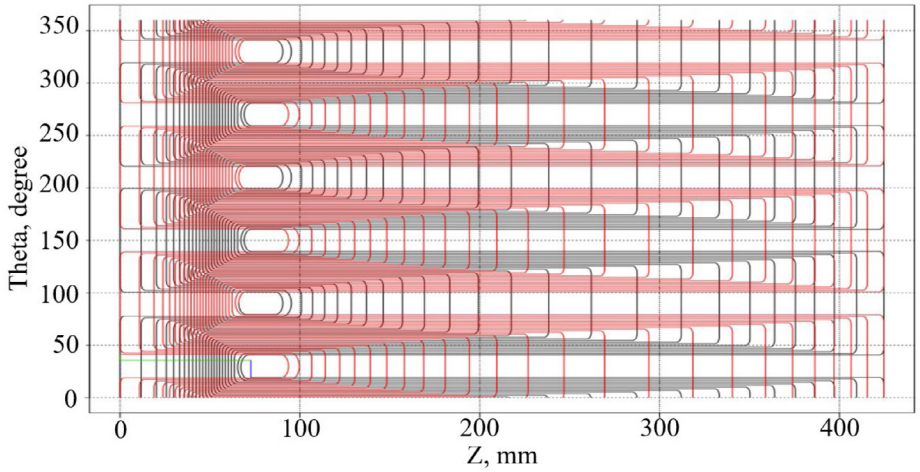

Fig. 20. Projected view of the sextupole leak field cancel magnet on the flat plane. The black line is the inner layer coil, and the red is the outer layer coil.. (For interpretation of the references to color in this figure legend, the reader is referred to the web version of this article.)

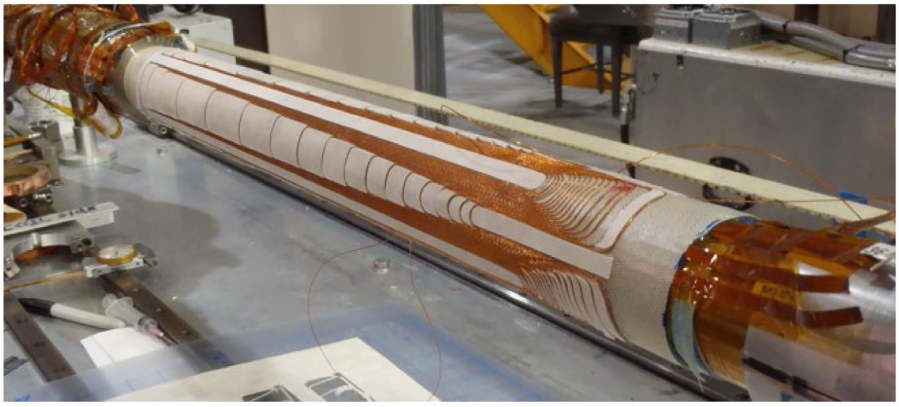

Fig. 21. Direct winding process of the QClLP octupole leak field cancel magnet in BNL.

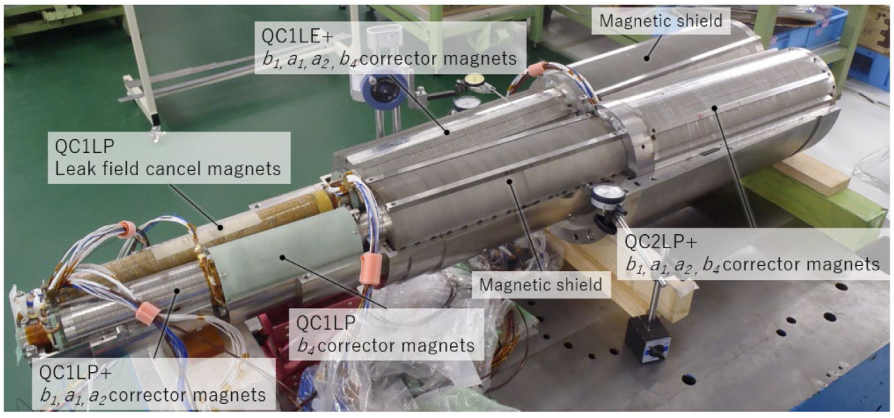

Fig. 22. Assembled QC1LP, QC1LE, QC2LP, the corrector magnets and the QC1LP leak field cancel magnets in the stainless steel support block.

the local field mapping measurement. Coils of 3 different radii were constructed because the beam pipe inner radii and the reference radii for QC1P, QC1E, QC2P and QC2E are different. The parameters of the harmonic coils, beam pipe and the reference radius are shown in Table 20. The beam pipe of QC1P is not round. It has the radius of 13.5 mm vertically and 10.5 mm horizontally. For the integral field measurements, the coil length was decided so that the difference between the measured integral field with the harmonic coil length and the calculated integral field of the whole magnet is smaller than 100 ppm. For the local field mapping measurements, the coil length was designed to be 20 mm long to measure the field change along the magnet axis especially in the coil ends. During the measurements, the longitudinal position of the center of the harmonic coil was measured with respect to the fiducial point on the system, and the coil center position was defined relative to the beam lines. For the magnetic field measurements in the beam lines, the special pipes were inserted into the cryostats besides of the real beam pipes. The harmonic coil radii

Table 17
Parameters of corrector magnets.

	Corrector type	L_c mm	L_{em} mm	R_c mm	T_c	L mH
QC1LP	a_1	316	281.1	21.5	36	0.76
	b_1	316	286.7	22.2	30	0.56
	a_2	316	299.5	22.9	19	0.46
	b_4	166	135.8	40.2	35	1.47
QC1RP	a_1	315	277.6	21.5	36	0.77
	b_1	295	247.2	22.5	38	0.76
	a_2	316	297.0	22.9	19	0.46
	b_4	166	135.8	40.6	36	1.37
	$a_3^{\#}$	160	118.9	42.1	48	1.69
QC2LP	a_1	445	351.1	49.0	84	7.38
	b_1	345	193.6	50.7	170	15.8
	a_2	446	409.3	49.7	40	3.36
	b_4	342	304.1	51.7	44	1.47
QC2RP	a_1	446	287.8	49.6	166	22.1
	b_1	364	197.3	52.1	74	16.9
	a_2	446	405.8	50.7	41	3.51
	a_3	81.3	57.0	52.1	31	0.36
QC1LE	a_1	406	357.5	29.8	51	2.52
	b_1	406	322.0	28.8	94	7.46
	a_2	406	383.1	30.5	26	4.53
	b_4	356	332.2	31.1	28	0.59
QC1RE	a_1	405	353.0	30.1	50	2.39
	b_1	406	321.5	29.1	94	7.39
	a_2	405	381.8	30.8	25	1.13
	a_3	322	304.0	31.4	18	0.69
QC2LE	a_1	566	467.7	55.4	93	10.7
	b_1	565	457.9	54.7	90	11.1
	a_2	566	520.7	56.3	46	5.92
	b_4	398	355.3	57.0	59	2.19
QC2RE	a_1	439	337.0	55.5	93	8.44
	b_1	507	398.8	54.8	90	9.01
	a_2	507	462.6	56.1	47	4.73
	a_3	319	287.4	56.5	33	2.52
QC12RE	b_3	392	340.8	53.5	62	30.8
QC12RP	b_3	222	186.6	37.1	42	2.08

L_c and L_{em} are the coil length and the effective magnetic length of each magnet, respectively. R_c is the coil center radius of the magnet. T_c is the turn number of the coil in each pole. L is the inductance.

Table 18
SC wire parameters of the corrector magnets.

Parameter	Value
SC wire material	NbTi
Wire diameter, mm	0.35
Cu/S ratio	1.0
Filament diameter, D_f, μm	5.4
No. of filaments, N_f	2113
RRR of Cu	181
Critical current I_c @ 4T, 4.22 K, A	154
@ 6T, 4.22 K, A	108

Table 19
Magnet parameters of the QC1RP/QC1LP leak field cancel magnet.

		L_c mm	R_c mm	T_c	L mH
QCS-R	Sextupole	415	21.8	22	0.404
	Octupole	389	23.1	18	0.306
	Decapole	392	25.1	16	0.244
	Dodecapole	348	26.4	12	0.142
QCS-L	Sextupole	423	22.1	22	0.409
	Octupole	388	23.2	18	0.309
	Decapole	392	25.1	16	0.239
	Dodecapole	359	26.4	12	0.146

were designed under these constraints. For QC1E, QC2P and QC2E, the reference radius (R_{ref}) is larger than the harmonic coil radius.

Table 20
Harmonic coil parameters.

	Beam pipe inner radius, mm	R_{ref}, mm	Integral meas.		Mapping meas.	
			L, mm	R, mm	L, mm	R, mm
QC1P	13.5(V), 10.5(H)	10	594.6	12.00	20.43	12.00
QC1E	17	15				
QC2P	35	30	695.0	25.04	20.39	25.04
QC2E	40	35	795.0	33.08	19.85	33.00

Table 21
Integral transfer functions of QC1 and QC2.

	I, kA	T.F. cal., T/kA	T.F. meas., T/kA	T.F. -U, T/kA	T.F. -D, T/kA
QC1LP	1.70	14.15	14.38	14.38	14.38
QC1RP	1.70	14.15	14.36	14.36	14.36
QC1LE	1.70	17.08	17.06	17.06	17.06
QC1RE	1.70	17.08	17.02	17.02	17.02
QC2LP	0.90	13.10	12.97	12.97	12.98
QC2RP	0.90	13.10	12.97	12.97	12.97
QC2LE	1.00	15.63	15.26	15.26	15.27
QC2RE	1.00	10.34	10.47	10.46	10.48

T.F. meas. is the average of the transfer functions during ramping the current up and down, T.F.-U and T.F.-D, respectively.

(b) Integral field measurements of QC1 and QC2

The variation of the integral transfer functions, T.F., of the quadrupoles with magnet current is shown in Fig. 23 with open circles and squares. The T.F. was measured without the combined solenoid field, and the measured values at the specific current are shown in Table 21.

The measured values of the integral T.F. of QC1LP and QC1RP at 1.7 kA are about 1.6% larger than the design value. This difference mainly comes from the magnetic length, which was calculated by the mapping measurement results. The measured lengths of QC1LP and QC1RP were 337.4 mm and 337.5 mm, and they correspond to the construction error of 1.14% and 1.17% with respect to the design length of 333.6 mm, respectively. From the lengths, the field gradients at I_d of QC1LP and QC1RP are 76.72 T/m and 76.59 T/m, and they are 0.45% and 0.28% larger than G_d, respectively. The magnetic field calculation of the quadrupole magnet was performed with the 3D model at room temperature. Therefore, the 0.28% larger field gradient of QC1RP is due to the thermal contraction of the magnet components from room temperature to 4 K, like 0.27% of stainless steel. The 0.45% error of QC1LP contains the 0.18% construction error without the thermal contraction effect. With the construction error, the evaluated SC coil radius is 45 μm smaller than the design.

As to the integral T.F. of QC1LE and QC1RE, there is 0.24% difference at 1.7 kA between these magnets. From the mapping measurement results, the effective magnetic length of QC1LE was 0.027% longer than the one of QC1RE, and the field gradient of QC1LE at the magnet center was 0.13% higher than QC1RE. In total, the difference is 0.16%. These errors correspond to 0.1 mm in the coil length and 40 μm in the coil radius. They are due to assembly errors during production of the magnets. Where is still 0.08% unknown difference in the integral T.F. of QC1LE and QC1RE, the possible cause is due to the temperature change of the harmonic coils at the measurements on the beam lines.

The QC1LE and QC1RE quadrupole magnets show reduction of the T.F. above 1.5 kA due to the magnetic saturation of the yokes. The reductions from 1.5 kA to 1.7 kA of QC1LE and QC1RE due to the solenoid fields were 0.009 T/kA and 0.017 T/kA, respectively. In the QC2 magnets, the magnetic saturation effect on the quadrupole field is negligible at the beam operation current.

The integral error multipole fields of the eight main quadrupole magnets are shown in Fig. 24. In each plot, the vertical axis is the normalized error field at the reference radius, R_{ref}, in units, and the horizontal axis is the multipole number. In the plots, a_n and b_n are

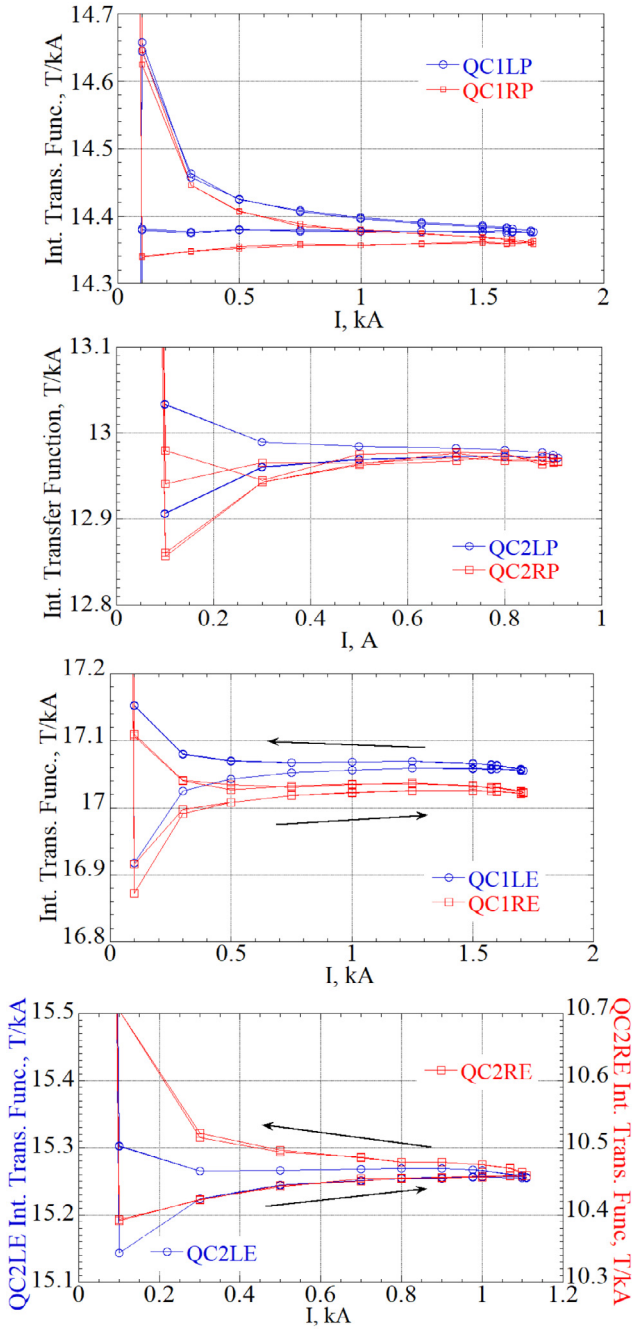

Fig. 23. Integral transfer function of QC1 and QC2 magnets without the combined solenoid fields.

the skew and normal components, respectively, and the fields with and without the solenoid fields are shown. Four quadrupole magnets of QC1 had good field quality. During the development of the proto-type QC1 magnets, we measured 5~6 units of the sextupole field [16]. The beam calculation showed that the sextupole field strongly reduced the beam lifetime [24]. This sextupole field was due to the dipole deformation caused by the wrong Young's modulus of the coil in the magnet cross section design. The cross sections of all magnets were redesigned. In the production QC1P and QC1E magnets, the sextupole field components were reduced to be smaller than 1.6 units.

The sextupole field components of the QC2P and QC2LE magnets are at the same level of the QC1 magnets. QC2RE shows a_3 of 18.9 units and a_4 of −8.1 units with the combined solenoid field in Fig. 24. The a_3 and a_4 reduced to 4.8 units and −0.61 units without the solenoid field, respectively. It was found from the field profile along the magnet axis in the mapping measurements that the a_3 and a_4 components were induced by the Belle II solenoid field at the surface of the iron block for supporting the magnets in the LHe vessel.

(c) Field mapping measurements of QC1 and QC2

The field profiles of the magnets were measured with the short harmonic coils of 20 mm long. As the example of the measured results, the B_2, A_3, B_3, A_4, and B_6 profiles at R_{ref} = 10 mm of QC1LP magnet are shown in Fig. 25. In the plot, the black line is the calculated profile, the red line with the close circles is the measured profile with the combined solenoid field, and the blue line with the crosses is the measured profile with no solenoid field. The symbols correspond to the measured values, and the horizontal axis is the distance from the IP. The position of the harmonic coil in the IR was measured with the laser tracker system with respect to the normal magnets on the beam lines. The harmonic coil was moved in steps of 5 mm which was measured with a magnetic scale of 10 μm resolution.

The B_2, B_4 and B_6 profiles show good agreement between the calculation and the measurements. The coil lead end is located on the IP side. In the ideal magnetic calculation, there are no B_3 and A_3 field components along the magnet axis, but in the real magnet, B_3 and A_3 within $\pm 1.5\times10^{-3}$ T existed in the magnet due to an assembly error of the coil. From the detail analysis of the B_2 profile by the measurement without the solenoid field, the B_2 center is located at Z=−934.50 mm with respect to the design at Z=−935 mm. When the Belle solenoid, ESL and ESR1 are excited, the magnetic forces act on ESL and ESR1. Therefore, the helium vessels, which contain ESL or ESR1 and the other SC magnets, are pushed outward from IP. The measured positions of all quadrupole magnets are shown in Table 22. The B_2 center of QC1LP moved from Z=−934.50 mm to Z=−936.94 mm by −2.44 mm as shown by Δ_{emf}. In the table, the position errors of the quadrupole field centers with respect to the design position are shown by Δ_d. The quadrupole magnets in the QCS-L front LHe vessel have large discrepancies with respect to the design position. This cause is a structural problem of the mechanical support components. The measured quadrupole positions were introduced into the beam optics used in operation of SuperKEKB. When the opportunity to open the LHe vessel is scheduled, the problem should be reduced.

In the integral measurements of QC2RE, the large differences in a_3 and a_4 between the results with and without the combined solenoid field are shown in Fig. 24. The source of these error fields was identified with the mapping measurements. Fig. 26 shows the field profiles of B_2, A_3 and B_3 along the QC2RE magnet axis by calculation and measurements with and without the solenoid fields. In each plot, the vertical and horizontal axes correspond to the field strengths at R_{ref} = 35 mm and the longitudinal position from IP, respectively. The measured longitudinal magnetic center is located at Z=2925 mm in the design. The magnet physical length is 560.7 mm, and the measured B_2 profiles show good agreement with the calculation. While A_3 and A_4 are zero in the design, the peaks of A_3 and A_4 in 2700 mm <Z< 2750 mm and 3100 mm <Z< 3150 mm are due to the construction errors in the coil ends. In 2550 mm <Z< 2700 mm and 3300 mm <Z< 3400 mm, there exist two peaks of A_3 and A_4. They are induced by the bore ends of the iron block which supports QC2RE in the LHe vessel. The shapes of the bore ends are not round to accommodate the SC lead cables, and cause the large A_3 and A_4 fields to be formed with the Belle II solenoid field.

(d) Integral field measurements of corrector magnets

All corrector magnets were measured by the harmonic coils at room temperature by BNL during construction, and after transporting them to KEK, they were measured at 4 K while being cooled by LHe at KEK. The field performance of all corrector magnets was confirmed independently before assembling in the cryostats. As final tests, the corrector magnetic fields were measured after installing the cryostats into the IR. In this paper, the measurement results at 4 K after being assembled into the cryostat are reported in Table 23. The field measurements were performed at the specified current with the current

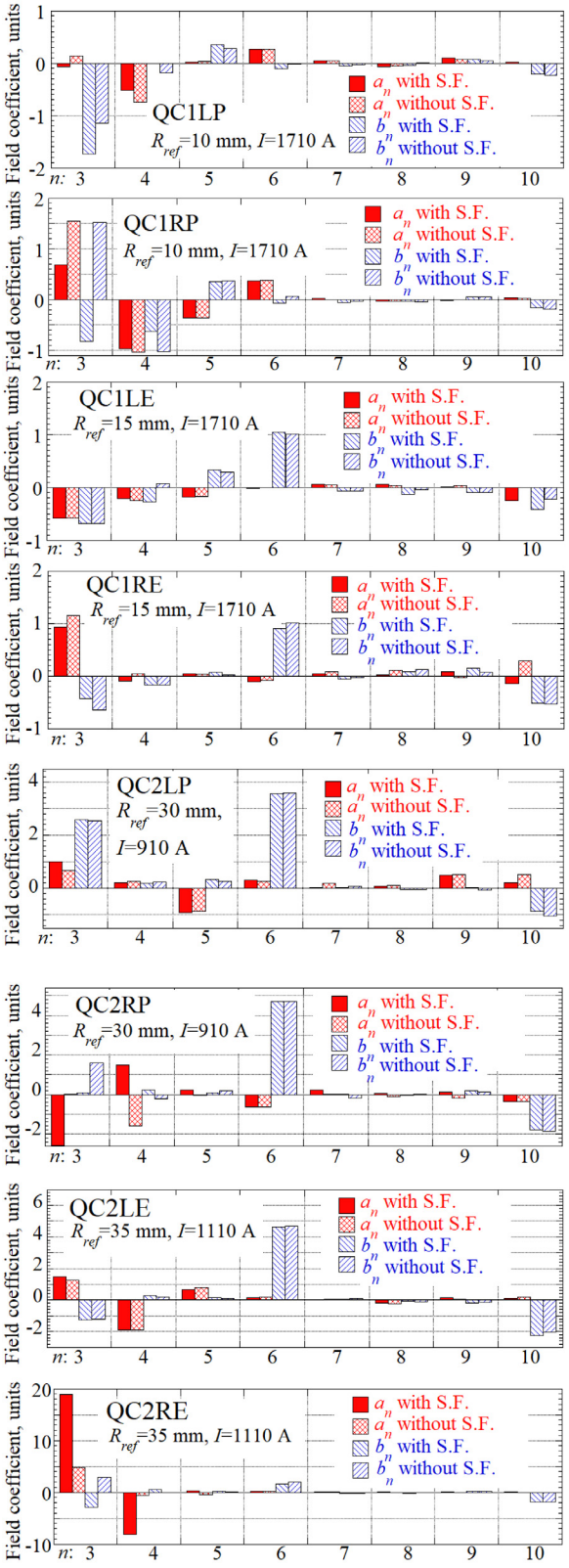

Fig. 24. Integral error fields of QC1 and QC2 magnets. In the plot, S.F. means the combined solenoid fields.

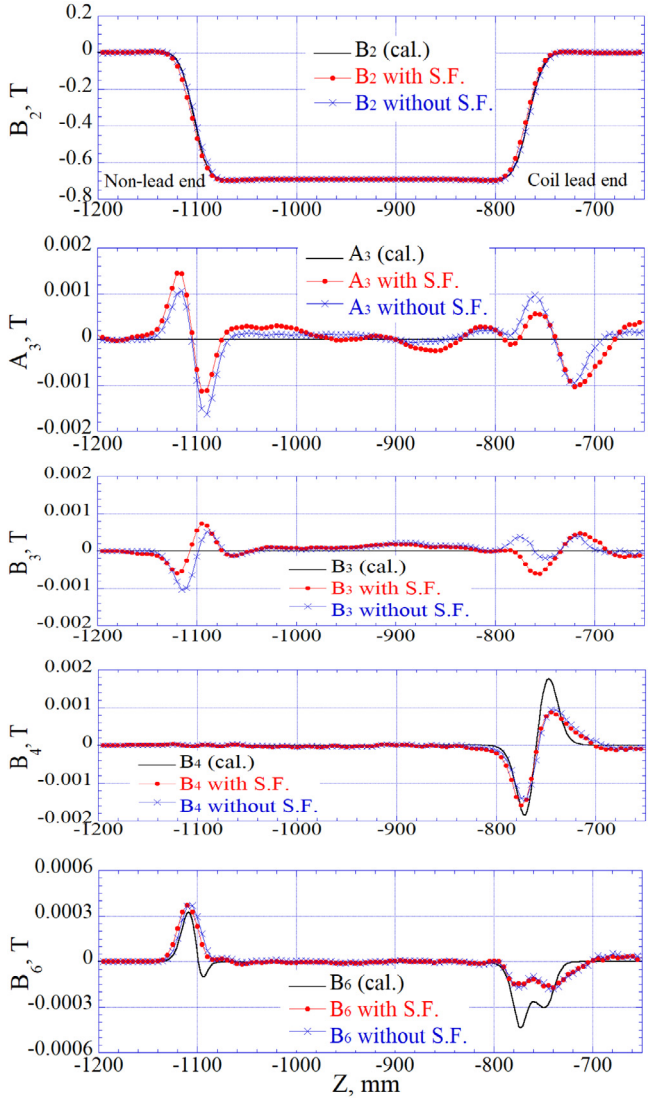

Fig. 25. Field profiles along QC1LP magnet axis.

Table 22
Movement of longitudinal magnetic center.

	Design mm	wo S. F. mm	w S. F. mm	Δ_{emf} mm	Δ_d mm
QC2LE	−2700	−2700.5	−2700.7	−0.2	−0.7
QC2LP	−1925	−1924.2	−1927.1	−2.9	−2.1
QC1LE	−1410	−1411.8	−1413.5	−1.7	−3.5
QC1LP	−935	−934.5	−936.9	−2.4	−1.9
QC1RP	935	935.0	935.9	0.9	0.9
QC1RE	1410	1409.8	1410.7	0.9	0.7
QC2RP	1925	1925.2	1926.1	0.9	1.1
QC2RE	2925	2925.8	2925.9	0.10	0.9

cycle of 0 A→60 A→0 A→−60 A→0 A after the preliminary cycle. In Table 23, the measured integral fields are shown at 60 A and −60 A. All corrector magnets besides the QC1RP a_3 corrector generated the required magnetic fields. In the measurements, the assembled unit of a_3 and b_4 correctors for QC1RP were rotated with 90 degrees, then the a_3 magnet functioned as the b_3 magnet.

The field hysteresis at 0 A during ramping the current up and down is shown as Δ_{his}. As an example of the measurement, the normal dipole field change of QC1LE b_1 corrector magnet with transport current is shown in Fig. 27. The field measurements were performed with and without excitation of QC1LE at 1577 A. For the b_1 magnet, Δ_{his} is −0.0014 T corresponding to 2.5% of the b_1 field at 60 A. Since the hysteresis effect on the fine beam tuning is quite history-dependent, the

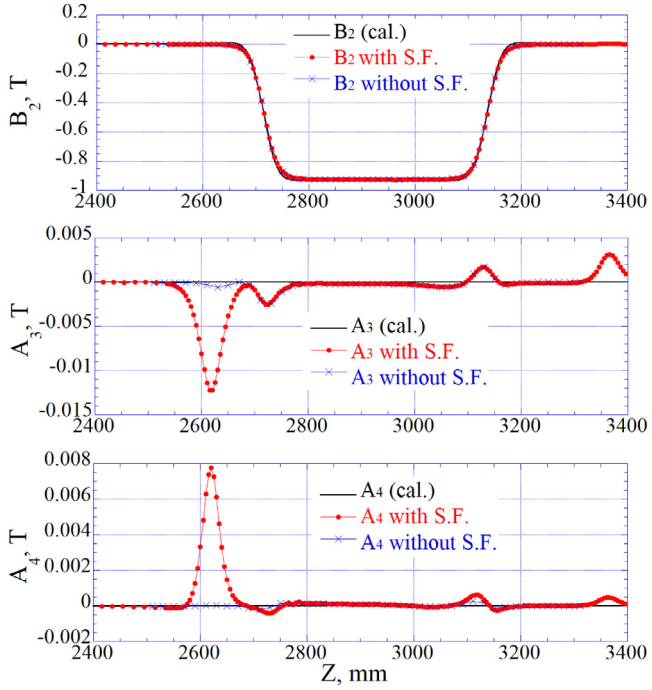

Fig. 26. Field profiles of B_2, A_3 and A_4 along the QC2RE magnet axis.

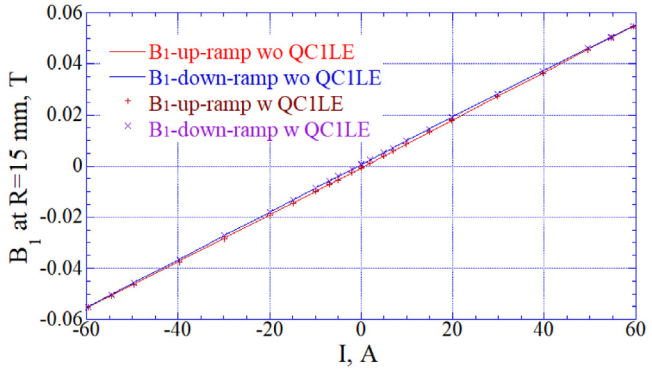

Fig. 27. Normal dipole field change of QC1LE b_1 corrector magnet with the transport current. The solid lines are the B_1 change without the QC1LE excitation, and symbols of plus and cross are the B_1 change with the QC1LE excitation.

method for changing the current to the target value is being studied to reduce the hysteresis effect on the beam operation.

(e) QC1P leak field cancel magnets.

The performance of the QC1P leak field cancel magnets was confirmed with the integral and the mapping harmonic coils. The integral field measurement results are summarized in Table 24. The exciting currents of QC1LP and QC1RP were 1625 A. The design currents of the leak field cancel b_3, b_4, b_5 and b_6 magnets were 40.10 A, 26.00 A, 17.20 A and 13.50 A, respectively. In the table, the integral B_3, B_4, B_5 and B_6 along the HER beam line from QC1LP and QC1RP are shown with and without excitation of the cancel magnets. The integral field of B_3 and B_4 were reduced to smaller than 1% of the original field. B_5 and B_6 were reduced to less than 10%.

The field profiles of the QC1P leak field cancel magnets were measured without and with excitation of QC1LP and QC1RP. Figs. 28 and 29 show the measured profiles in QCS-L and QCS-R at R_{ref} = 10 mm. The signs of the multipole field components between the measurements in QCS-L and QCS-R are opposite due to the accelerator coordinate system. In both figures, the left plots show the field profiles along the beam line with the b_3, b_4, b_5 and b_6 corrector magnets at the design currents, and the right plots correspond to the combined field profiles with the corrector magnets, QC1LP and QC1RP at 1625 A. The leak fields of the normal field components along the HER beam line are almost canceled out.

Table 23
Measured integral field of corrector magnets.

	Type	@ 60A	@ -60A	Δ_{his}@ 0A	θ mrad
QC1LP	a_1	0.0177	−0.0178	−0.0006	15.0
	b_1	0.0148	−0.0144	−0.0005	25.6
	a_2	0.806	−0.803	−0.038	−31.0
	b_4	294.5	−292.6	13.4	−1.7
QC1RP	a_1	0.0174	−0.0175	0.0006	10.7
	b_1	0.0157	−0.0161	−0.0006	11.9
	a_2	0.797	−0.799	−0.043	5.2
	b_4	−264.8	267.1	14.2	−14.3
	b_3	−9.55	9.41	0.21	−4.4
QC1LE	a_1	0.0327	−0.0321	−0.0011	−16.2
	b_1	0.0554	−0.0554	−0.0014	−6.1
	a_2	0.932	−0.931	−0.055	−6.1
	b_4	724.3	−723.6	23.9	−1.2
QC1RE	a_1	−0.0313	0.0313	0.0011	3.8
	b_1	0.0550	−0.0550	−0.0014	2.4
	a_2	0.888	−0.889	−0.051	−4.0
	a_3	−22.60	22.69	1.29	4.1
QC2LP	a_1	0.0355	−0.0355	−0.0009	3.9
	b_1	0.0409	−0.0409	−0.0007	8.6
	a_2	0.640	−0.640	−0.031	9.3
	b_4	−159.5	159.4	9.18	10.2
QC2RP	a_1	−0.0578	0.0578	0.0010	−0.1
	b_1	0.0423	−0.0423	−0.0008	−0.1
	a_2	0.630	−0.629	−0.032	5.9
	a_3	−1.585	1.662	0.138	28.0
QC2LE	a_1	0.0400	−0.0400	−0.0010	2.3
	b_1	0.0442	−0.0442	−0.0011	3.8
	a_2	0.753	−0.752	−0.035	−8.0
	b_4	142.0	−142.0	−6.70	−4.4
QC2RE	a_1	−0.0310	0.0310	0.0011	−6.6
	b_1	−0.0353	0.0353	0.0012	11.2
	a_2	0.600	−0.600	−0.034	−7.6
	a_3	6.493	−6.446	−0.322	−12.6
QC1-2RE	b_3	55.51	−55.49	−0.089	−45.3
QC1-2RP	b_3	−28.03	28.03	0.051	−4.5

In the table, the units of the integral field are Tm for a_1 and b_1, T for a_2, T/m for a_3 and b_3 and T/m^2 for b_4. Δ_{his} is the difference between the measured values at 0 A during ramping the transport current up and down. θ (mrad) is the roll angle of the corrector field with respect to the quadrupole field.

The difficulty of these leak field cancel magnets is in the alignment accuracy with respect to QC1LP and QC1RP. Especially, the error in the azimuthal direction easily induces a skew field component. In the as-built system, the skew field components were measured, and they are shown in Table 24. From the optics calculation, the A_3 field components, which have a strong influence on the beam operation, are confirmed to be corrected by the a_3 magnet in QC1RE.

4.2. Solenoid field profile measurement along the beam lines

The solenoid field profile along each beam lines was measured with 3 axis Hall sensors. The measured solenoid field profiles are shown in Fig. 30, with the calculated profiles. In the figure, B_z is the axial field component along the beam line, and B_r is the radial field component. The measured profiles consist of the data measured by the accelerator group (shown by dots) and the Belle II group (open squares). The field profiles from the accelerator group were measured with a commercial 3 axis Hall probe. The probe was moved in 20 mm steps along the beam lines. It scanned the magnetic fields in three dimensions. The probe has an error of 0.5% for magnetic fields higher than 2 T as the device specification. Fine calibration of the probe is going on with

Table 24
Measured integral leak fields at R_{ref} = 10 mm.

Multipole coefficient	QCSL, Tm		QCSR, Tm	
	without canceling	with canceling	without canceling	with canceling
b_3	3.36×10^{-3}	2.32×10^{-5}	-3.53×10^{-3}	1.27×10^{-5}
b_4	-7.58×10^{-4}	-2.83×10^{-6}	8.02×10^{-4}	4.39×10^{-6}
b_5	1.57×10^{-4}	3.66×10^{-6}	-1.67×10^{-4}	-3.73×10^{-6}
b_6	-2.98×10^{-5}	7.8×10^{-7}	3.24×10^{-5}	2.35×10^{-6}
a_3	-2.42×10^{-4}	-3.88×10^{-4}	-2.52×10^{-4}	-4.93×10^{-4}
a_4	-5.88×10^{-5}	-1.16×10^{-4}	4.94×10^{-5}	1.71×10^{-4}
a_5	-1.48×10^{-5}	-1.48×10^{-5}	6.26×10^{-6}	-8.31×10^{-6}
a_6	1.88×10^{-5}	1.48×10^{-5}	-4.31×10^{-6}	-1.09×10^{-6}

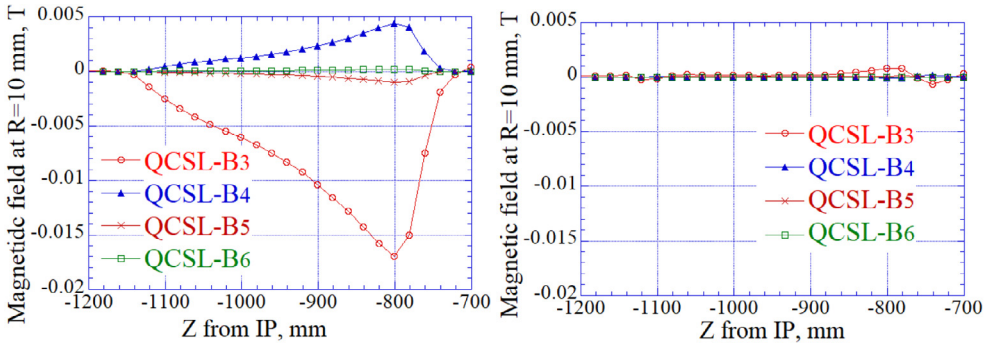

Fig. 28. Field profiles of the b_3, b_4, b_5, b_6 magnets for QC1LP (left) and the canceled leak field of QC1LP by these magnets (right).

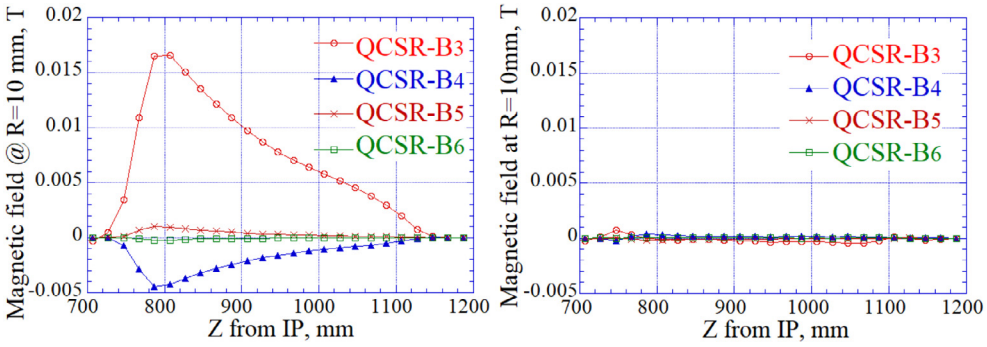

Fig. 29. Field profiles of the b_3, b_4, b_5, b_6 magnets for QC1RP (left) and the canceled leak field of QC1RP by these magnets (right).

the ANL 4 *T* MRI solenoid with FNAL and ANL under the U.S.-Japan Science and Technology Cooperation Program in High Energy Physics. The field profile near the IP was provided by the Belle II group, and it was measured with a set of 3 axis Hall sensors. The sensors were supplied by CERN [25] under the coordination of the DESY-Belle II group. The calculated and measured solenoid field profiles show good agreements in plots. The excitation currents of the ESL, ESR1 and ESR2/3 were decided using the measurements and the calculation. The operation currents of ESL, ESR1 and ESR2/3 are 390 A, 450 A and 151 A, respectively.

From the detailed comparison of measurement and calculation of the solenoid field profiles, the measured field profiles of 0.6 m < Z < 1.4 m for QCS-R and −1.4 m < Z < −0.6 m for QCS-L have shifts along Z axis by 0.4 ± 0.5 mm and −2.3 ± 0.5 mm with respect to the calculated field profiles, respectively. The result shows that ESR1 and ESL were moved along the Belle II solenoid axis by the EMFs which were induced by interference between the solenoid fields of ESL, ESR1 and Belle-II. The magnets of QC1L/RP, QC1L/RE and QC2L/RP are locked to the solenoid bores of ESL and ESR1, and then the quadrupole magnets and the solenoids move in the same way. As shown in Table 22, the average movements of the three quadrupole magnets by the EMFs (Δ_{emf}) in each side are 0.9 mm and −2.3 mm for QCS-R and QCS-L, respectively. These results give close agreement with each other, indicating that the helium vessels with all these magnets are moved by the EMFs.

4.3. Quadrupole magnets alignment measurements by single stretched wire (SSW)

The quadrupole magnetic field center and the roll angle were measured with the SSW system which was developed by FNAL under the U.S.-Japan Science and Technology Cooperation Program in High Energy Physics. The Be-Cu wire of diameter 0.1 mm was set on the design beam line through two cryostat bores. The wire was stretched between two stands as shown in Fig. 31. Each stand was placed in the rear of the magnet cryostat and on the cryostat support stage. The stands can perform vertical and horizontal wire translations to determine magnet position and can vary the tension of the wire so that sag effects can be removed. The stands also have fiducials which are calibrated with respect to the wire position, so that the wire position at the stands can be aligned with respect to the design beam positions with a laser tracker measurement system. The SSW measured the quadrupole magnet center positions and the mid-plane field angles of four SC quadrupole magnets with respect to each design beam line and the horizontal plane. The measurements were performed under the collision magnetic field conditions with and without the Belle II solenoid and the compensation solenoids. The measured results are shown in Table 25. Δx and Δy are the horizontal and vertical displacements of the quadrupole field centers from the design line and $\Delta\theta$ is the roll angle error of the quadrupole field mid-plane.

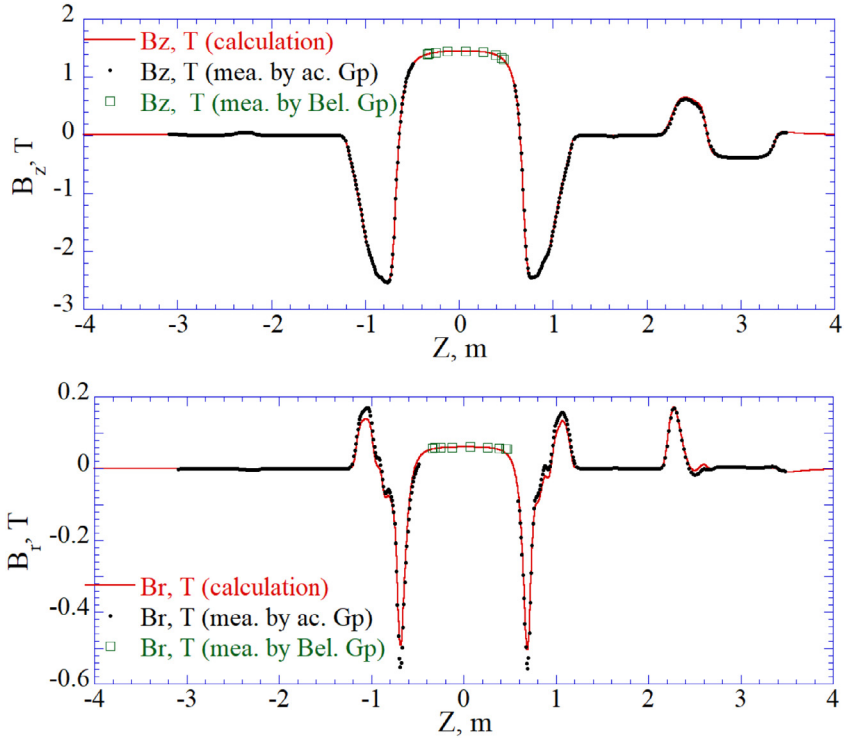

Fig. 30. Solenoid field profiles on the HER beam line measured by Hall probes.

Table 25
Measured displacement of quadrupole field center and roll angle error of quadrupole field plane.

	Δx, mm		Δy, mm		Δθ, mrad
	w S. F.	wo S. F.	w S. F.	wo S. F.	w S. F.
QC1LE	−0.21	−0.16	−0.29	−0.56	−1.6
QC2LE	0.13	0.11	−0.54	−0.68	−1.5
QC1RE	0.25	0.14	−0.37	−0.54	0.0
QC2RE	0.08	0.07	−0.58	−0.63	−0.7
QC1LP	−0.03	−0.14	−0.21	−0.38	−1.7
QC2LP	−0.31	−0.41	−0.68	−0.83	−4.0
QC1RP	0.64	0.69	−0.30	−0.43	2.0
QC2RP	0.43	0.45	0.04	−0.19	−1.7

In the table, Δx and Δy are the displacement in the horizontal and vertical directions and $\Delta\theta$ is the roll angle error.

As shown in Table 25, there are discrepancies between Δx and Δy with and without solenoid fields. The maximum is 0.27 mm in Δy of QC1LE. They are due to the EMF produced by the Belle II solenoid field, the compensation solenoids and the magnetic components in the helium vessels. Beam optics studies confirmed that the off-centers of the quadrupole fields were adjusted by the corrector magnets and by tuning the beam orbit.

Concerning the roll angles of the quadrupole magnets, the maximum error was −4.0 mrad for QC2LP. This angle error was induced by a magnet assembly error in the helium vessel. The assembly error is evaluated to be in the range of ±0.2 mm on the outer circumference of this magnet. All errors can be corrected with the skew quadrupole corrector magnets.

5. Magnet cryostat and cryogenic system

The magnet cryostats are key components to keep the operation of the superconducting magnets stable under the Belle II solenoid field at 1.5 T, the heavy electrical magnetic forces on the magnets and the magnetic components in the helium vessels, and a quite tight space constraint to keep the magnets at temperature less than 4.75 K in design. In the following section, the designs of the cryostats and the measurements on the mechanical and thermal loads are described.

5.1. Cryostat system design

The cryostat consists of a magnet cryostat, a service cryostat, a cryogenic transfer tube and a support table. Fig. 32 shows the top and side views of the QCS-R cryostat, and the horizontal and vertical cross sections. The QCS-L cryostat has almost the same configuration as QCS-R. The cryostat parameters are listed in Table 26.

In the magnet cryostat, the superconducting magnets are assembled in two LHe vessels (the front vessel in IP side and the rear vessel in non-IP side). QC1RP, QC2RP, QC1RE and ESR1 are assembled in the front vessel, and QC2RE, ESR2 and ESR3 are in the rear vessel. For protecting the Belle II detector components from the radiation by the beams, radiation shields of tungsten alloy whose density is 18 g/cm^3 are installed in the front vessels. The total weights of the radiation shields are 231 kg and 1271 kg for QCS-L and QCS-R, respectively. The magnet cryostat and the service cryostat are connected by the pipe, and the cryogenic transfer tubes from the helium refrigerator are connected at the service cryostat. The current leads are mounted on the service cryostat. The leads for the quadrupole magnets and the solenoids are a conventional type and cooled with vaporized helium gas. The leads for the corrector magnets are a compact assembled unit where 8 leads are embedded. REBCO HTS tape is soldered along the low temperature part of the lead [26,27]. Additional leads are connected to ESL and ESR1, individually, for tuning the field profile along the solenoid magnet to cancel the Belle II solenoid field integrally. In total, the QCS-L and QCS-R service cryostats have 41 and 66 leads, respectively.

The weights of the QCS-L and QCS-R magnet cryostats are 3137 kg and 4647 kg, respectively. Each cryostat is cantilevered toward the IP from its support table. The material of the support table is SS400 (in JIS) because the tables work as the magnetic shield of the fringe field from the Belle II solenoid to the conventional magnets which were set inside of this table and close to the detector.

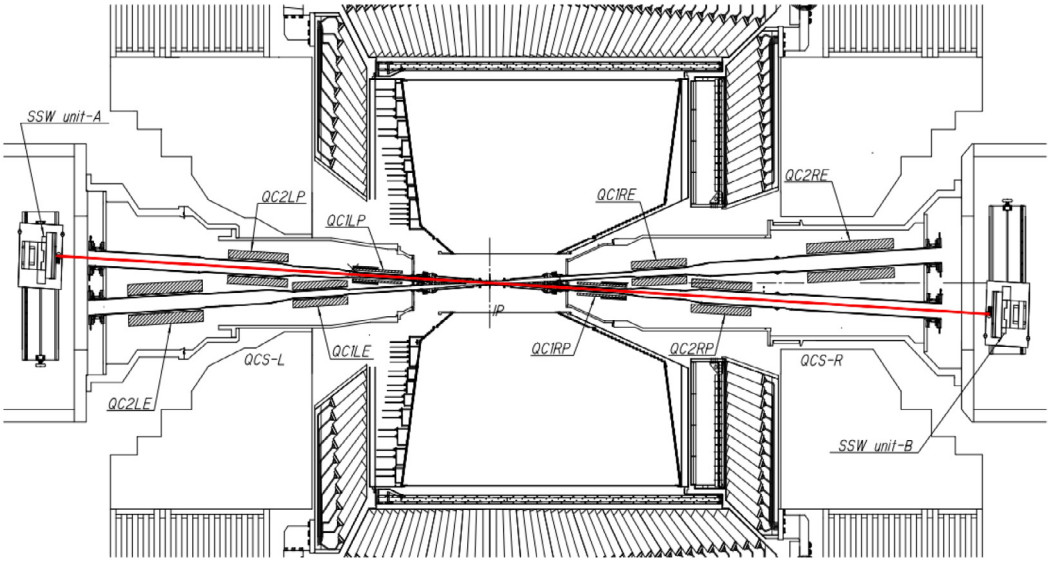

Fig. 31. A schematic layout of the SSW measurement system.

Table 26
Cryostat parameters.

Parameters	QCS-L	QCS-R
Magnet cryostat		
Vacuum vessel length	2724 mm	3287 mm
Vacuum vessel max. dia.	ϕ1100 mm	ϕ638 mm
Vacuum vessel mass	1570 kg	1472 kg
4 K cold mass		
Front vessel length	1585.4 mm	1604.5 mm
Front magnets and others	949 kg	805 kg
Tungsten radiation shield	231 kg	1271 kg
Rear vessel length	700 mm	794.7 mm
Rear magnets and others	342 kg	1063 kg
80 K thermal radiation shield	45 kg	36 kg
Service cryostat		
Vacuum vessel length	2757 mm	2757 mm
Vacuum vessel height	917 mm	917 mm
Vacuum vessel wide	900 mm	863 mm
Vacuum vessel mass	2523 kg	2501 kg
80 K thermal radiation shield	79 kg	77 kg
He gas-cooled current leads		
Conventional leads	5 pairs	5 pairs
Compact 8 terminal leads	5 units	7 units
Additional lead for ESL and ESR	1	2[a]
Support table		
Length	3810 mm	3810 mm
Wide	1540 mm	1540 mm
Mass	6279 kg	6061 kg
Total cryostat system length	6533 mm	7087 mm
Total cryostat mass	12550 kg	15000 kg

[a]2 leads in the compact unit of 8 terminal leads are used as the additional lead for ESR.

Table 27
Mechanical loads of the suspension rods of the front vessels.

	QCS-L		QCS-R	
	MW	EMF	MW	EMF
ES excitation	1260 kg	−52.6 kN	2076 kg	35.7 kN
Stress in rod	161 MPa		206 MPa	
ES non-excitation	1260 kg	57.3 kN	2076 kg	−23.5 kN
Stress in rod	174 MPa		152 MPa	

In the table, MW and EMF mean the weight of the cold mass and the electro-magnetic force on the front helium vessel, respectively. The sign of EMF is plus for the direction from QCS-L to QCS-R.

5.2. Cryostat mechanical design

The helium vessels are supported by a suspension system of eight titanium alloy (Ti-6Al-4V) rods [28,29]. In Fig. 33, the system for the front vessel of the QCS-R cryostat is shown. The lengths of the rods are 75.5 mm and 108 mm in the front (shown by A in the figure) and back (B) sides, respectively. The rods are designed to have a tilt angle so that the center between the rod supporting points on the helium vessel does not change when the vessel is cooled down from room temperature to 4 K and the rods have temperature gradients along the rod axes. The angles of the front and back rods at room temperature are 20.16 degree and 20.14 degree, respectively, and after cool-down to 4.5 K, they are changed to 18.83 degree and 19.72 degree, respectively. With thermal contraction during cool-down, the quadrupole magnet centers change as shown in Fig. 33. The QC1RP center changes 2.35 mm and 0.12 mm in the axial and horizontal directions, respectively. The vertical displacement by the thermal contraction is negligible. The magnets and cryostat components in the helium vessels at 300 K are designed so that the magnet centers at 4.5 K are positioned on the beam lines.

The rods are designed to withstand the forces and the weight of the helium vessel. When the Belle II solenoid is excited, ESL and ESR1, the EMFs act on ESL and ESR1 due to the Belle II solenoid field. The calculated EMFs on ESL and ESR1 are 52.6 kN and 35.7 kN, respectively. The front helium vessels are pushed outward from the IP by the EMFs. On the other hand, if ESL and ESR1 are not excited due to a magnet quench or similar event, the magnetic components in the vessels are drawn into the IP. The EMFs on QCS-L/R vessels are 57.3 kN and 23.5 kN, respectively. The calculated values are summarized in Table 27. The cross-section areas of the rods for QCS-L/R are 182.3 mm^2 and 81 mm^2, and the maximum stress in the rods is 174 MPa and 205 MPa, respectively. The stress is much smaller than the yield strength of the titanium alloy at room temperature (825 MPa).

5.3. Cryostat thermal design

The magnet cryostats are thermally designed so that the superconducting magnets are cooled with single phase liquid helium (LHe) for stable operation during beam operation. The two cryostats are cooled by individual helium refrigerators as shown in Fig. 2. The refrigerator can supply subcooled LHe of 20 g/s at 4.35 K and 0.16 MPa to the cryostat and the cryogenic transfer tube. To keep the cooling helium in single phase liquid the maximum heat load to the cryostat and the

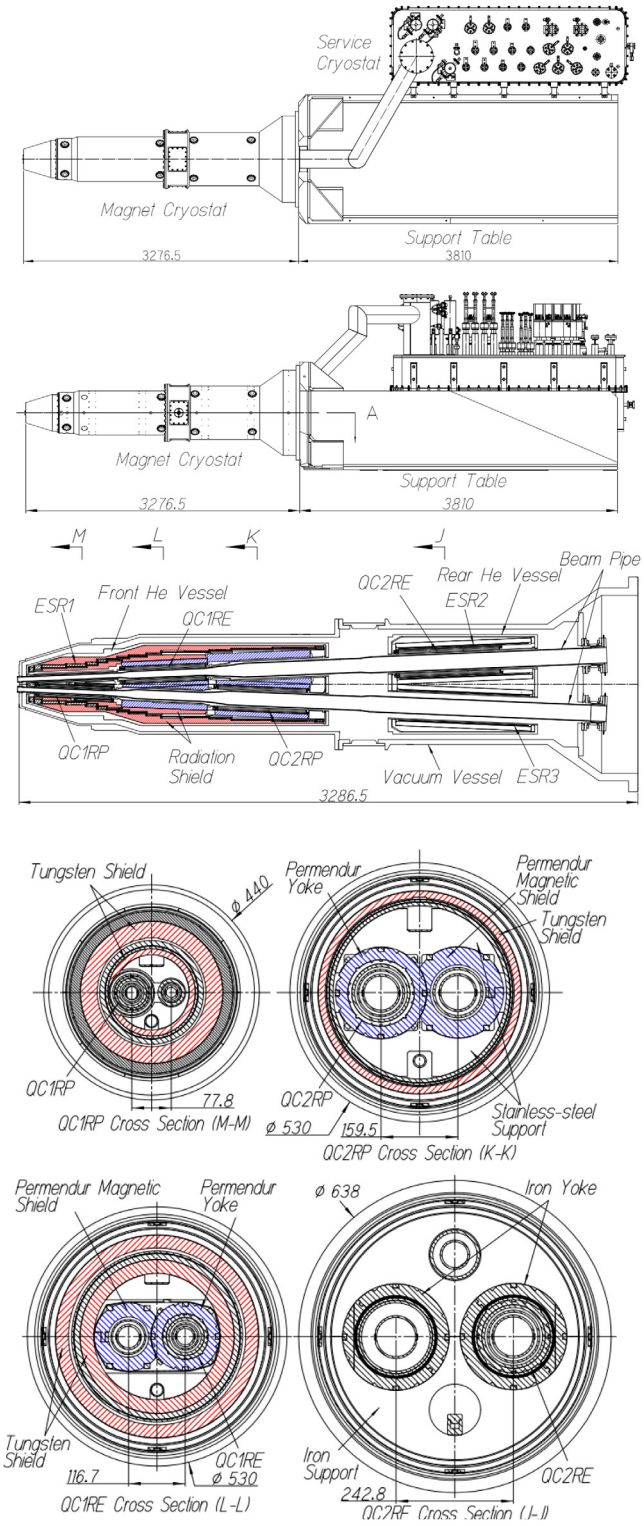

Fig. 32. External view of QCS-R magnet cryostat and the cross sections of the magnet cryostat. The upper two figures show the whole cryostat viewed from above and from the side, respectively. The middle figure is the horizontal cross section of the magnet cryostat, and the downside pictures are the vertical cross sections of the magnet cryostat at each quadrupole magnet center.

tube is 32.8 W. The design thermal loads for the two cryostats are summarized in Table 28. In the table, the load components of increasing the single phase LHe temperature are those of the suspension rods and the thermal radiation in the magnet cryostats, and those of the transfer tube, valves, and the instrument wires in the service cryostats. The summations of these components are 26.1 W and 25.3 W for QCS-L and QCS-R, respectively. Both loads are below the allowable heat loads.

Table 28
Design heat loads of the cryostats at 4 K.

	QCS-L	QCS-R
Magnet cryostats		
Suspension rod	9.7 W	5.8 W
Thermal radiation	6.6 W	10.1 W
Sub-total	16.3 W	15.9 W
Service cryostat		
Thermal radiation	1.9 W	2.1 W
C.L. pipe	11.5 W	12.5 W
T.T. + V	6.0 W	6.0 W
Instrument wire	3.8 W	3.4 W
He gas for C.L.	1.00 g/s	1.03 g/s
Sub-total	23.2 W + 1.00 g/s	24.0 W + 1.03 g/s
Total	40.5 W + 1.00 g/s	40.7 W + 1.03 g/s

where, C.L., T. T. and V mean the current lead, the cryogenic transfer tube and the cryogenic valve, respectively.

In this thermal design, while the outer surfaces of the helium vessels are covered with the thermal shields cooled by liquid nitrogen and a multi-layer insulation system, the bores for the beam pipes do not have the thermal shields because of the limited space between the bores and the beam pipes. In Fig. 34, the horizontal cross section of the front part of the QCS-R cryostat is shown. The helium vessel has two bores at 4 K for accommodating the beam pipes. The right figure shows the QC1RP cross section. The minimum distance between the bore (4.5 K) and the beam pipe (300 K) is 3.5 mm. The beam pipe, which is heated by synchrotron radiation, is kept at room temperature with circulating water. The corrector magnets are directly attached to the outer surface of the bore pipe. The corrector magnets of a_1, b_1 and a_2 are shown as the hatched areas in Fig. 34. The QC1RP magnet is assembled around the corrector magnets, and the space between QC1RP and the corrector magnets is used as a cooling channel containing LHe. To reduce the heat load to the helium vessel bores by thermal radiation, the outer surfaces of the beam pipes are wrapped with 5 layers of superinsulation (SI) sheet. The inner surface of the bore (SS316L) is mirror-processed and coated with aluminum by vapor deposition. The emissivity coefficient of this bore surface is evaluated below 10 K to be smaller than 0.02 [30], and the heat load due to the thermal radiation is reduced by more than 50%, compared to the surface of SS316L. In this thermal condition, the temperature of the innermost layer of the correction magnet is calculated to be less than 5 K.

The QCS-L and QCS-R service cryostats have 16 and 17 ports for the current leads, respectively. The port pipes are thermally anchored to the thermal shields cooled by liquid nitrogen, and the heat loads through the pipes of QCS-L and QCS-R are 11.5 W and 12.5 W, respectively. The current leads are cooled partly by the LHe remaining after cooling the magnets and partly by the evaporated helium gas. The total heat loads of the QCS-L and QCS-R cryostats are calculated to be 40.5 W + 1.00 g/s and 40.7 W + 1.03 g/s, respectively.

5.4. Cryogenic system

Each cryostat is cooled with an individual cryogenic system. The system consists of a helium refrigerator, a sub-cooler, a helium compressor, helium gas tanks and a liquid nitrogen storage tank. The specific cooling power of the refrigerator is 250 W at 4.4 K. The refrigerators are repurposed from the TRISTAN [31,32] and KEKB final focus SC magnet systems [33]. Each refrigerator has a sub-cooler which has been modified from the ones made for TRISTAN and KEKB, and cools two-phase liquid helium at 0.161 MPa and 4.75 K to a sub-cooled condition at 0.161 MPa and 4.35 K [34]. The cryogenic parameters are summarized in Table 29. Due to the heat load between the sub-cooler and the magnet-cryostat, the LHe temperature rises to 4.6 K. In typical operation conditions of the cryogenic system (at 4 Nov. 2020), the cryogenic parameters are listed in Table 30.

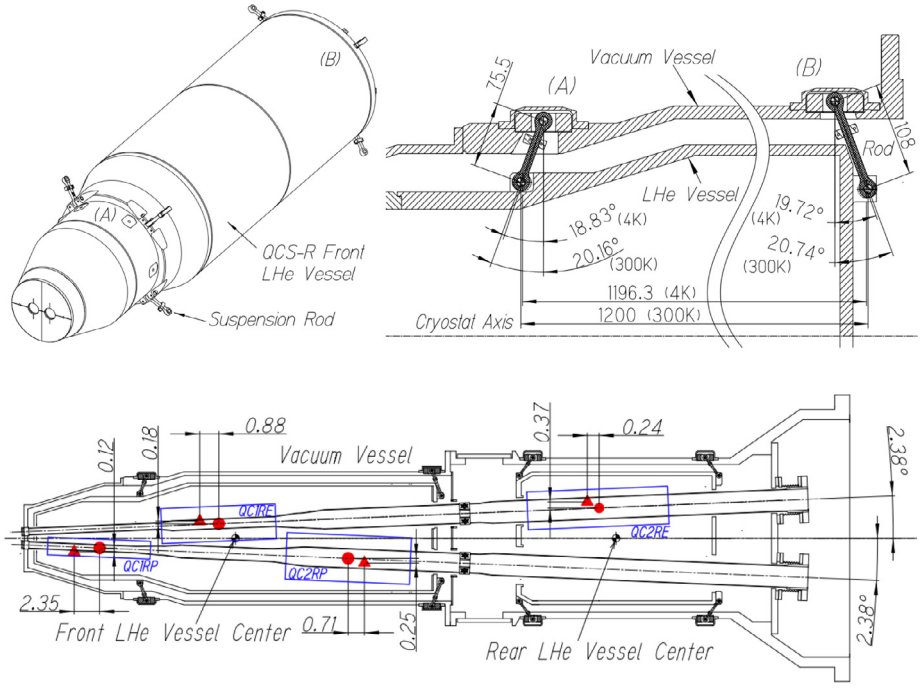

Fig. 33. Suspension rods of the QCS-R front helium vessel (upper left), the rod design (upper right) and the quadrupole magnet center changes due to cool-down (lower). The quadrupole magnet centers at 300 K and 4 K are shown with triangle and circle symbols, respectively. The position changes are shown in mm.

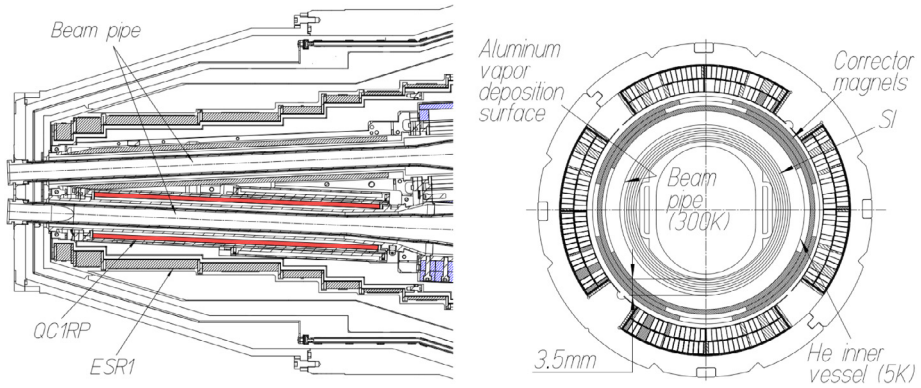

Fig. 34. Cross sections of the front part of the QCS-R magnet cryostat. The left figure shows the horizontal cross section of the QCS-R cryostat where the QC1RP magnet is placed. The right figure is the QC1RP cross section.

6. Beam operation and magnet quench

The beam operation of SuperKEKB with the final focus SC magnets started in May 2018. The β_y^*s of the beams at the IP were squeezed to 0.8 mm by June 2020, compared to the design target of 0.3 mm. During this beam operation, the SC magnets had quench events induced by the beams as shown together with the β_y^* squeezing process in Fig. 35. In the early stages of the operation period, the QCS system had 15 quench events in April, 2018. Because of the nested configuration of the quadrupole magnet and the corrector magnets, in each quench event, more than one magnet quenches. On April 23rd, 2018, the collimators [35] were adjusted following beam tuning studies and the number of the quench events induced by the beam was greatly reduced. The recovery time from a magnet quench to beam operation is typically two hours for the quadrupoles and the correctors. For the case of ESL and ESR1, the stored energy is larger than the other magnets as shown in Table 13, and then the recovery time from a quench to beam operation was more than 12 h in 2018 and 2019. In particular, ESR1 has 814 kJ of stored energy at 450 A, and the ESR1 quench led to large liquid helium evaporation and the shutdown of the helium compressor by the interlock in the cryogenic system. Since then, the recovery time has been reduced to 6 h by improving the quench recovery process of the system. To protect ESR1 against the voltage and temperature rises induced by the quench, the six cold diodes are connected to the solenoids [36,37]. As noted above, the frequency of beam induced quenches was reduced due to the improvement of the beam tuning process and the adjustment of the collimators. By increasing the cooling power of the refrigerator, we are trying to further reduce the recovery time from a magnet quench to beam operation.

7. Conclusion

The superconducting final focus system of SuperKEKB has been designed and built. The system has operated for three years so far. The superconducting magnet system is made up of 55 superconducting magnets. All magnets are required to meet stringent performance requirements and to be operated under very heavy work conditions. The system has already contributed to squeezing β_y^* to 0.8 mm, which is the smallest value in the world, but not yet the design value. This process of beam squeezing to the design is continuing now with studies

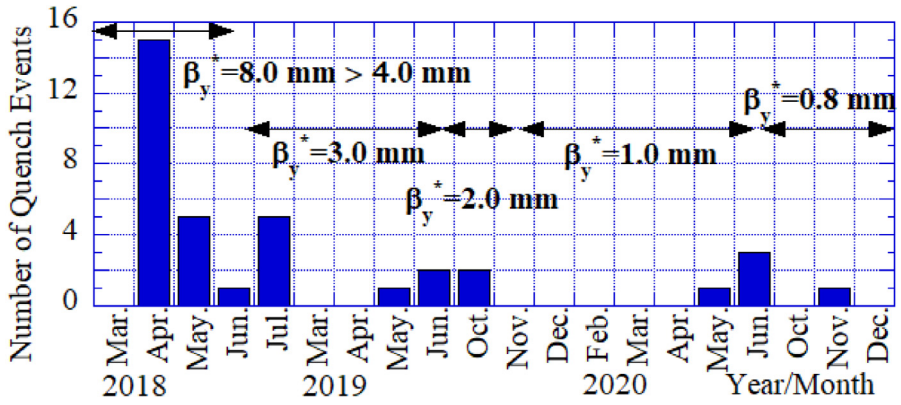

Fig. 35. History of quench events of the QCS system.

Table 29
Parameters of the cryogenic system.

Parameters	Value
Refrigerator	Claude cycle (two turbines)
Cooling power @ 4.4 K	250 W (using LN_2)
Helium compressor	Screw compressor
Maximum flow rate	1250 Nm^3/h (73.6 g/s)
Electric power	250 kW
Sub-cooler	Heat exchanger, H.X.
H. X. (Cu pipe)	ID 15.5 mm, OD 18.4 mm, L 41.4 m
LHe reservoir	200 L
He at the inlet of H.X.	4.75 K, 0.161 MPa, 25 g/s
He at the outlet of H.X.	4.35 K, 0.161 MPa, 25 g/s
GHe tank	2.06 MPa, V=20 m^3×2 units
GHe tank for quench	0.395 MPa, V= 3 m^3
LN_2 storage tank	9800 L

Table 30
Operation parameters of the system.

Parameters	QCS-L	QCS-R
Compressor flow rate	57.7 g/s	54.9 g/s
GHe press. at outlet	1.6 MPa	1.6 MPa
Refrigerator, Sub-cooler		
He flow rate to turbine	29.4 g/s	27.2 g/s
He flow rate to cryostat	25.2 g/s	23.6 g/s
Magnet cryostat		
Helium temperature at magnets	4.55 K	4.60 K
Helium pressure	0.06 MPa	0.06 MPa
Total flow rate for cooling C. L.	1.28 g/s	1.29 g/s
Cooling power margin at 4.5 K	26 W	16 W

For this table, pressure is the relative to atmosphere.

and tuning the collimator system, the radiation shield against the beam background to the particle detectors and the accelerator system including the injector.

In the following, we would like to summarize the technical issues of the superconducting final focus system of the SuperKEKB accelerator.

(1) Main quadrupole magnets: Eight superconducting quadrupole magnets were constructed. Because the field qualities of QC1P and QC1E depend on the assembly errors and have a strong impact on beam collisions and operation, prototypes were constructed and studied. The results from the prototypes were fed back to the designs of the production QC1P and QC1E magnets and to the designs of the QC2P and QC2E magnets. The eight magnets have sufficient field quality for beam operation. The magnetic field performance was measured with harmonic coils in the beam lines to confirm the quality for the beam operation. From the measured results, the error fields mainly came from the positioning errors of the SC cable in the coil ends, which have many tiny end spacers because the eight quadrupole magnets were short, and the ratio of the length of the coil ends to the length of the whole coils was over 15%.

(2) Compensation solenoids: Because of the large beam crossing angle and the very tight space in the cryostats, the solenoids were designed in a circular cone as a whole and then separated into small coils. The magnetic field profiles of the solenoids were measured by the Hall probe and reproduced the calculated field. After the magnetic field measurements by the Hall probe, the excitation currents of the solenoids were adjusted so that the integral solenoid fields along the beam lines were less than 0.01 Tm. An unusual technical difficulty arose from the solenoid inductance, which changed with excitation current because the solenoids had magnetic components in their bores. This feature made the power converter difficult to control.

(3) Corrector magnets and QC1P leak field cancel magnets: In this extremely complex final focus system and tight space, the unique solution for the design of the corrector system was to use multi-layered magnets wound with thin SC wire. The corrector magnets were successfully constructed by the BNL direct winding machines. The a_1, b_1 and a_2 magnets operated from the beginning of the beam operation. Although they were quenched by the early irregular beams, this problem was resolved with tuning the collimators and the beam control after dedicated studies. The a_3 magnets are already used in tuning the beams, and the b_3 and b_4 magnets will be used in the coming beam operation. In the a_3 magnet of QC1RP, an error in assembly in the He vessel was found after construction was completed. The error will be corrected in the future. With regard to the QC1P leak field cancel magnets, the magnets might have rotation errors with respect to the QC1P leak field from the magnetic field measurements. The process of canceling the leak field was designed assuming no winding and assembly errors. Considering the complex operating conditions and the required precision in the assembly process, one cancel magnet should be separated into two magnets, skew and normal, which would be excited independently.

(4) Magnetic field measurements: We used three types of measurement systems for measuring the magnetic fields in the beam lines and under the expected operating conditions. The short harmonic coils and the Hall probe showed the precise magnetic field profiles along the beam lines. We detected the magnet movement due to the EMFs and the error magnetic fields in the support iron block of QC2RE. The SSW system developed by FNAL was the only technique to measure directly the magnetic centers and roll angles of the main quadrupole magnets in the fully constructed IR with Belle-II.

(5) Cryostat and cryogenic system: The magnet cryostats are the key components for operating the SC magnets stably under the hard-edged mechanical and thermal conditions: the magnet

support with the large EMFs on the SC magnets and magnetic components, the quite tight space for the thermal insulation, the specification of the magnet alignment with the EMFs, and thermal contraction of all components with the beam crossing angle. Over the last three years, the cryostats provided a steady operating condition for exciting the magnets subject to the large EMFs due to interference between the solenoid field profiles of ESL, ESR1 and Belle-II. As to the cryogenic system, the cooling power margin of the system at beam operation was increased to 30 W~35 W at 4.5 K after improving the operating parameters of the helium expansion turbines. The cryogenic systems are now maintaining the very stable performance needed for exciting magnets during beam operation.

(6) Beam operation: So far during beam operation at β_y^* of 0.8 mm, the collimators have functioned for reducing magnet quenching and beam background noise to the detectors. To attain β_y^*s =0.3 mm, we will start improving the radiation shields, the collimator system and the beam optics beginning with beam operation in October 2021 and continuing during the following accelerator shutdown period. SuperKEKB has already entered a new region of high energy particle accelerator performance. In the process of squeezing β_y^* and increasing the luminosity, the present final focus system is being studied as one component in the accelerator system. Improvement and modification of the final focus system and the other accelerator components are being discussed for future operations.

Declaration of competing interest

The authors declare that they have no known competing financial interests or personal relationships that could have appeared to influence the work reported in this paper.

Acknowledgments

The authors would like to show our deep appreciation to all members of the KEKB accelerator review committee. We would like to express our sincere thanks to Mr. T.-H. Kim in Mitsubishi Electric Corp. for completing the magnets and cryostats. The project was supported by the US–Japan Science and Technology Cooperation Program in High Energy Physics. We are extremely grateful to the late Dr. Satoshi Ozaki for continuously supporting this project. All authors approved the version of the manuscript to be published.

References

[1] SuperKEKB design report, https://kds.kek.jp/event/15914/.
[2] S. Kurokawa, et al., KEK-B: The KEK B-factory, Nucl. Instr. Meth. A 499 (2003) 1–233.
[3] T. Abe, et al., Achievements of KEKB, PTEP 2013 (2013) 03A001.
[4] P. Raimondi, 2nd superB meeting, frascati, 2006.
[5] N. Ohuchi, et al., Design of the superconducting magnet system for the SuperKEKB interaction region, in: Proc. of NA-PAC'13, Pasadena CA, USA, Sept. 2013, pp. 759–761.
[6] N. Ohuchi, et al., Design and construction of the SuperKEKB QC1 final focus superconducting magnets, IEEE Trans. Appl. Supercond. 25 (3) (2015) 4001202.
[7] N. Ohuchi, et al., Design and construction of the QC2 superconducting magnets in the SuperKEKB IR, in: Proc. IPAC'16, Busan, Korea, 2016, pp. 1174–1176.
[8] B. Parker, et al., Direct wind superconducting corrector magnets for the SuperKEKB IR, in: Proc. of IPAC'12, New Orleans, USA, 2012, pp. 2191–2193.
[9] B. Parker, et al., Superconducting corrector IR magnet production for SuperKEKB, in: Proc. of NA-PAC'13, Pasadena CA, USA, Sept. 2013, pp. 1241–1243.
[10] B. Parker, et al., The SuperKEKB interaction region corrector magnets, in: Proc. of IPAC'16, Busan, Korea, 2016, pp. 1193–1195.
[11] H. Yamaoka, et al., Solenoid field calculation of the SuperKEKB interaction region, in: Proc. of IPAC'12, New Orleans, USA, 2012, pp. 3548–3550.
[12] Y. Makida, et al., Development of a superconducting solenoid magnet system for the B-factory detector (BELLE), in: Advances in Cryogenic Engineering, 43A, 1998, pp. 221–228.
[13] Nippon Steel Corporation, High-strength nonmagnetic steel.
[14] Tohoku Steel Co., LTD, Cobalt-iron soft ferromagnetic alloy.
[15] B. Parker, et al., BNL direct wind superconducting magnets, IEEE Trans. Appl. Supercond. 22 (3) (2012) 4101604.
[16] N. Ohuchi, et al., Design and construction of the proto-type quadrupole magnets for the SuperKEKB interaction region, in: Proc. of NA-PAC'13, Pasadena CA, USA, Sept. 2013, pp. 1232–1234.
[17] M. Tawada, et al., Design study of final focusing superconducting magnets for the SuperKEKB, in: Proc. of IPAC2011, San Sebastian, Spain, Sept. 2011, pp. 2457–2459.
[18] N. Ohuchi, et al., Magnetic field measurement system for the SuperKEKB final focusing superconducting magnets, in: Proc. of IPAC2014, Dresden, Germany, Jun. 2014, pp. 2693–2695.
[19] Y. Arimoto, et al., Magnetic field measurement for superconducting-quadrupole magnets of final-focus system for SuperKEKB, in: Proc. of IPAC2016, Busan, Korea, 2016, pp. 3771–3773.
[20] Lakeshore, 3-channel Gaussmeter Model 460.
[21] J. DiMarco, J. Krzywinski, MTF Single Stretched Wire System, Tech. Rep. MTF-96-0001, Fermi National Accelerator Laboratory, 1996.
[22] J. DiMarco, et al., Field alignment of quadrupole magnets for the LHC interaction regions, IEEE Trans. Appl. Supercond. (ISSN: 1051-8223) 10 (1) (2000) 127–130, http://dx.doi.org/10.1109/77.828192.
[23] Y. Arimoto, et al., Magnetic measurement with single stretched wire method on SuperKEKB final focus quadrupoles, in: Proc. of IPAC2019, Melbourne, Australia, 2019, pp. 432–435.
[24] H. Sugimoto, et al., Design study of SuperKEKB interaction region optics, in: Proc. of IPAC2014, Dresden, Germany, Jun. 2014, pp. 950–952.
[25] F. Bergsma, H. Boterenbrood, BsCAN3, a Modular 3D Magnetic-Field Sensor System with CANopen Interface, CERN/Nikhef, 2013, http://www.nikhef.nl/pub/departments/ct/po/html/Bsensor/BsCAN3.pdf.
[26] Z. Zong, et al., Development of a compact HTS lead unit for the SC correction coils of the SuperKEKB final focusing magnet system, Nucl. Instr. Meth. A 830 (2016) 279–286.
[27] Fujikura, FYSC-SCH HTS REBCO tape.
[28] Y. Morita, et al., Liquid helium cryostat for the TRISTAN superconducting insertion quadrupole magnets, in: Advances in Cryogenic Engineering, Vol. 37A, 1992, pp. 551–558.
[29] N. Ohuchi, et al., Cryostats for the KEKB IR superconducting magnets, in: Advances in Cryogenic Engineering, Vol. 45A, 2000, pp. 787–794.
[30] J. Chaussy, et al., Reduction of evaporation rate by use of metallic adhesive tape, Cryogenics (1976) 617–618.
[31] K. Tsuchiya, et al., Superconducting Magnet System for the TRISTAN Low-Beta Insertion, in: Proc. of the 2nd European Particle Accelerator Conference, Nice (France), 1990, pp.1151-1153.
[32] K. Tsuchiya, et al., Cryogenic system of the superconducting insertion quadrupole magnets for TRISTAN main ring, in: Advances in Cryogenic Engineering, Vol. 35, 1990, pp. 941–948.
[33] K. Tsuchiya, et al., Final-focus superconducting magnet system for the interaction region of KEKB, in: Proc. of the 6th European Particle Accelerator Conference (EPAC98), Stockholm, 22-27, 1998, pp. 2038-2040.
[34] N. Ohuchi, K. Tsuchiya, Studies on a heat exchanger producing subcooled liquid helium, in: Advances in Cryogenic Engineering, Vol. 41A, 1995, pp. 225–231.
[35] T. Ishibashi, et al., Movable collimator system for SuperKEKB, Phys. Rev. Accelerators Beams 23 (2020) 053501.
[36] X. Wang, et al., Design and performance test of a superconducting compensation solenoid for SuperKEKB, IEEE Trans. Appl. Supercond. 26 (4) (2016) 4102205.
[37] X. Wang, et al., Quench characteristics of a superconducting compensation solenoid for SuperKEKB, IEEE Trans. Appl. Supercond. 29 (5) (2019) 4100305.